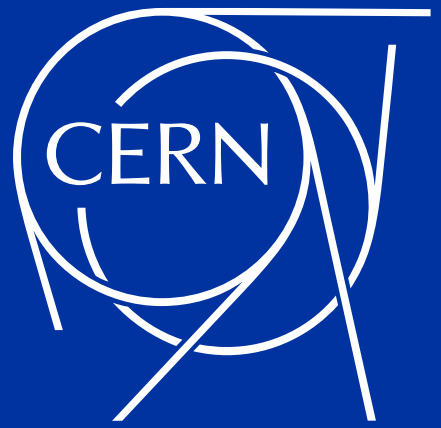

Diffusive models and chaos indicators for non-linear betatron motion

Carlo Emilio Montanari

BE Seminar

17 November 2023

Home Institute Supervisor– prof. Armando Bazzani
(Alma Mater Studiorum – University of Bologna)

CERN Supervisor – dr. Massimo Giovannozzi

Overview

- **Problem** –modelling the **long-term transverse beam dynamics to improve the beam lifetime**.
  - Beam losses in high-energy circular accelerators are a **critical limitation** in present and future machines;
  - Understanding **beam-halo formation** is critical for the development of higher energy and intensity machines;
  - Promising **non-linear diffusive models**, based on **stochastic Hamiltonian frameworks**, were proposed;
- **Contribution 1** – defining an **optimal collimator scan** protocol for measuring the transverse beam diffusion coefficient.
  - Collimators in the LHC are movable blocks that are used to **remove particles at excessive amplitude**;
  - By moving the jaws following an **original protocol**, we can measure the diffusion coefficient;
- **Contribution 2** – reconstruction of the diffusion coefficient from available LHC Run2 data.
- **Contribution 3** – application of **chaos indicators** on single-particle tracking.
  - Tracking simulations are used to inspect numerous accelerator lattice configurations;
  - **Novel chaos indicators** can be used to efficiently detect chaotic structures in the phase-space, and investigate their **connection to diffusive-like behaviours**;

The accelerator model

- Relativistic charged particle in EM field;
- Magnetic elements, 2n-polar elements composing the lattice of the accelerator;
- Negligible synchrotron radiation (hadron accelerators only), particle energy can be considered constant – a Hamiltonian description is possible;
- Courant-Snyder formalism, the co-ordinates are normalized over the “reference” circular trajectory, which enables us to study the longitudinal and transverse displacements from such reference;
- Within this formalism, we focus on studying the **transverse-beam dynamics and the transverse-beam distribution.**

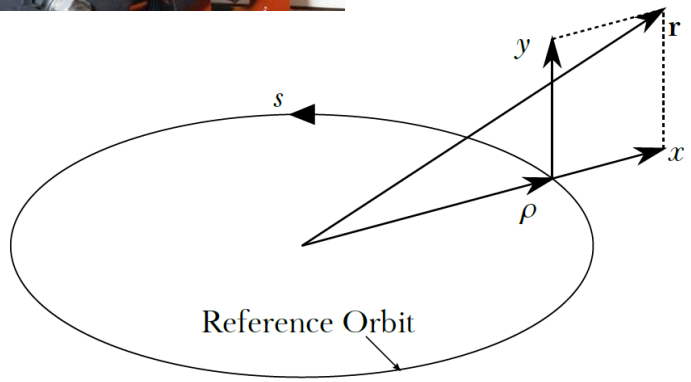

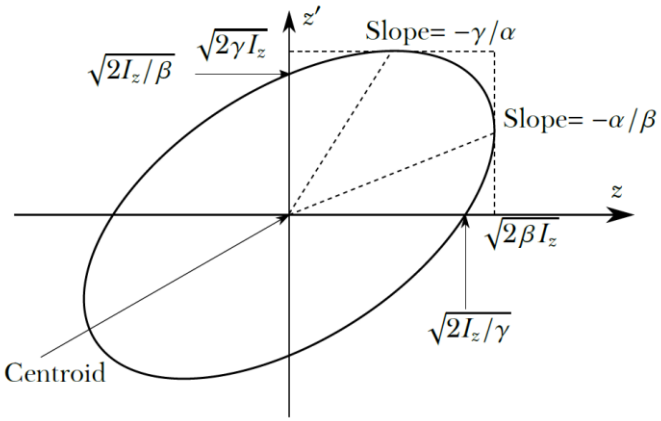

Theoretical foundation

This line of work sparks from the following considerations:

- Many studies higlighted how the **evolution of Dynamic Aperture** (i.e., the phase space region where stable motion occurs) can be described as a function of the number of turns, in a form **related to the Nekhoroshev Theorem**, that is:

$$DA(N) = \rho_* \left(\frac{\kappa}{2e}\right)^{\kappa} \frac{1}{\ln^{\kappa}\frac{N}{N_0}} \; ;$$

- Recent studies also explored the possibility of describing the evolution of the beam distribution using a **diffusive framework**, also related to Nekhoroshev Theorem;

- Experimental measurements of LHC halo dynamics at different amplitudes are available, as well as some first estimates of diffusive behavior.

The diffusive framework in a nutshell (1/3)

We describe the particle motion in terms of a **stochastic perturbed Hamiltonian system**

$$H(\theta, I, t) = H_0(I) + \xi(t) H_1(\theta, I)$$

- $H_0(I)$ linear part of the magnetic lattice (up to quadrupole magnet components);
- $H_1(\theta, I)$ non-integrable, non-linear part that causes the phase-space inhomogeneities;
- $\xi(t)$ stochastic noise with zero mean and unit variance.

From this initial setup, we can make use of important theorems in perturbed Hamiltonian mechanics such as:

1. The Kolmogorov-Arnold-Mooser theorem (KAM);
   - If a system is subjected to a weak nonlinear perturbation, some of the invariant tori are deformed and survive;
2. The **Nekhoroshev theorem/estimate**;
   - There is an upper estimate to the stability time of an orbit, dependent on the initial amplitude;

The diffusive framework in a nutshell (2/3)

The latest scale-law proposals for Dynamic Aperture are fully based on the Nekhoroshev theorem and provided good result in the extrapolation of long-term DA evolution.

From these promising results, the natural development of this framework is the construction of a more generalised beam-tail evolution model.

Starting from the perturbed Hamiltonian $H(\theta, I, t)$, we can apply the **Averaging Principle**, and describe the beam distribution $\rho(I, t)$ as the solution of the **Fokker-Planck equation**:

$$\frac{\partial \rho}{\partial t} = \frac{\varepsilon^2}{2} \frac{\partial}{\partial I} \left(D(I) \frac{\partial \rho}{\partial I} \right)$$

Where $D(I)$ is the **angular average of the non-integrable part** $\left\langle \left(\frac{\partial H_1}{\partial \theta} \right)^2 \right\rangle_\theta$, which can be estimated via optimal remainders and by means of the Nekhoroshev theorem.

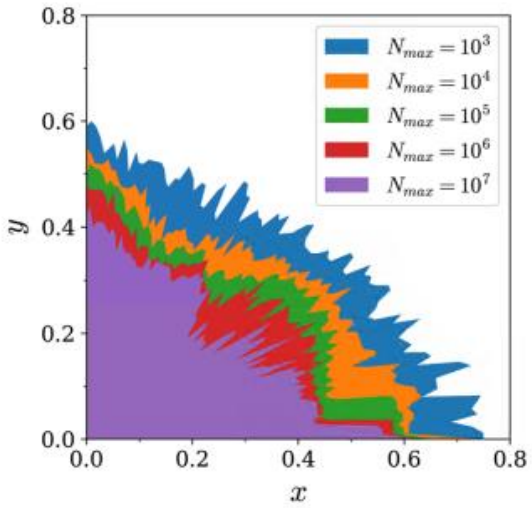

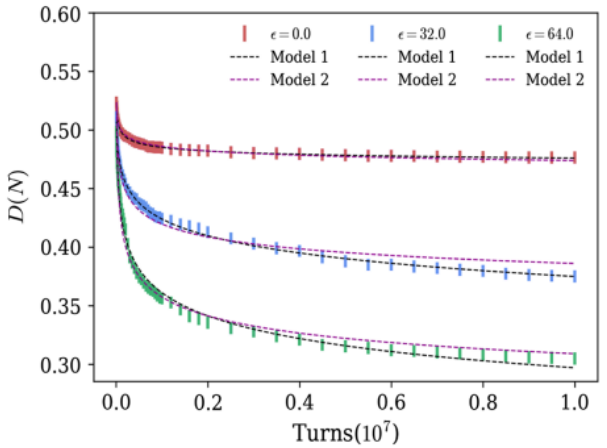

FIG. 2. Evolution of the dynamic aperture as a function of turn number (markers) for the three values of the ϵ parameter used in Fig. 1. The error associated with the numerical estimate of the DA are also shown, together with the results of the DA Model 1 and 2 (lines). The other two models are not shown here as they provide results very similar to those of Model 2.

The diffusive framework in a nutshell (2/2)

- The Nekhoroshev Theorem suggests the functional form

$$D(I) = \exp\left[-2\left(\frac{I_*}{I}\right)^{\frac{1}{2\kappa}}\right]$$

- Three distinct regions:
  - a stable core ($I/I_* < 0.6$);
  - a slow diffusion region ($0.6 < I/I_* < 1.0$);
  - a fast diffusion region ($I/I_* > 1.0$).

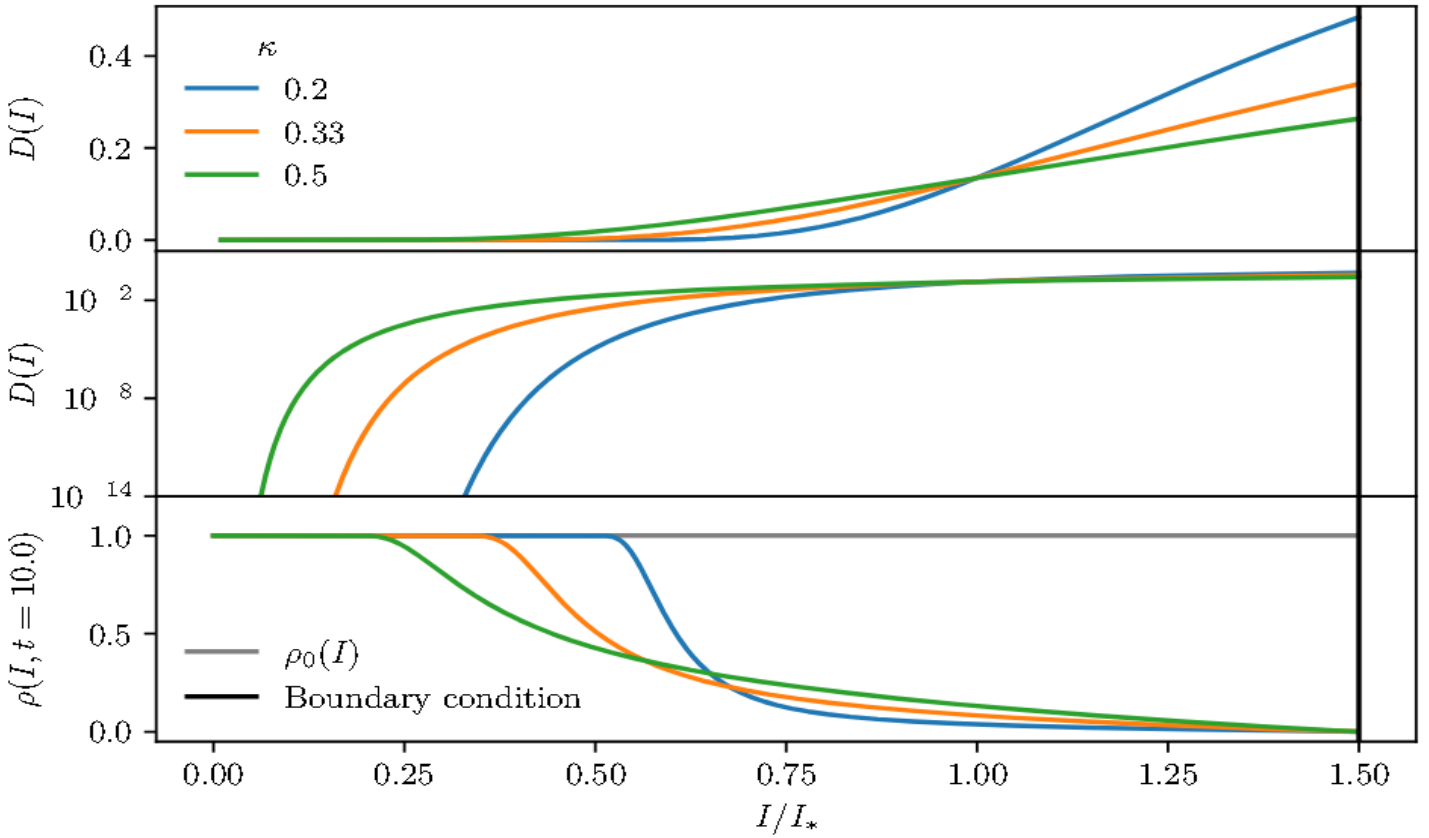

Reconstructing a Nekhoroshev-Like $D(I)$ from experimental data

(Specific) Important components

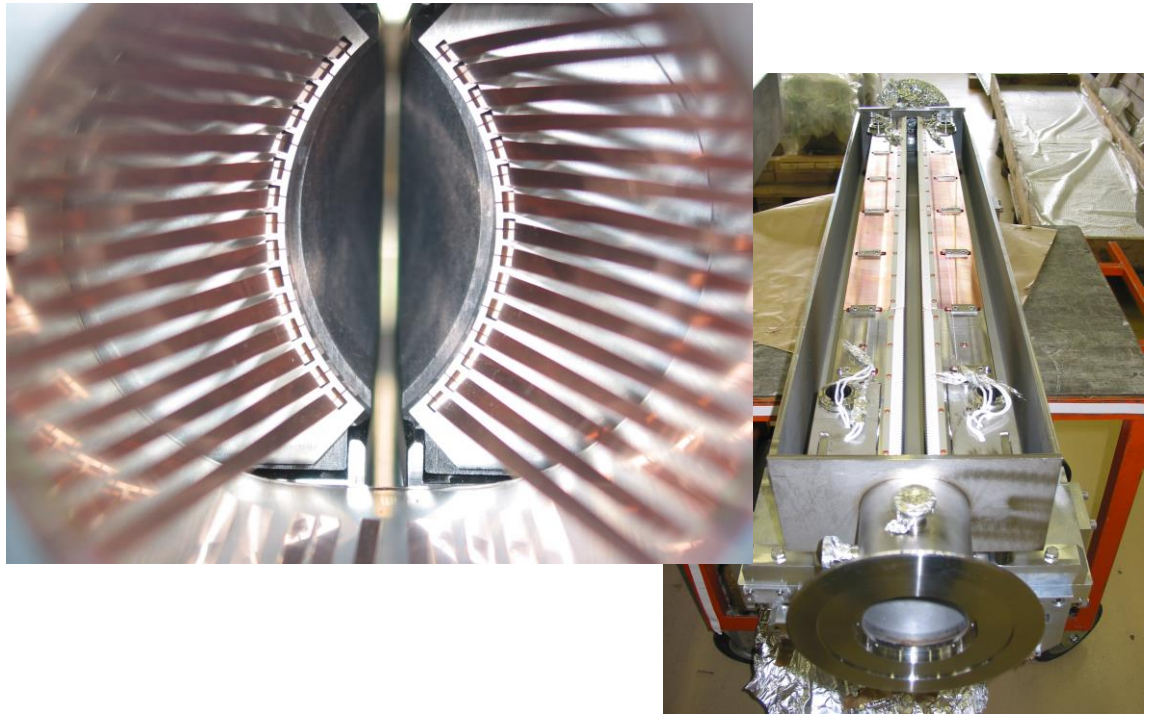

Collimator jaws

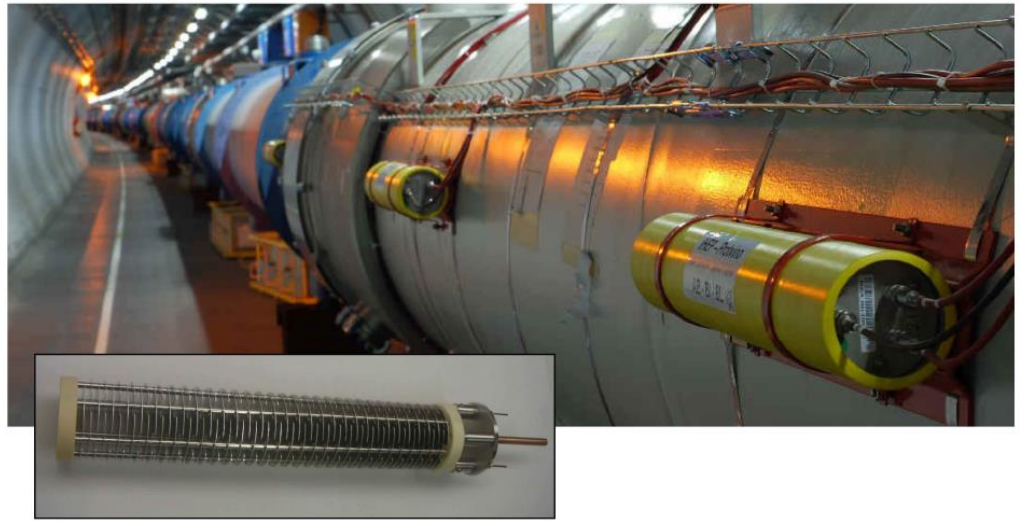

Beam Loss Monitors
(BLMs)

Reconstructing $D(I)$ from collimator scans

- If we **assume** that a beam distribution follows a Fokker-Plank equation with Nekhoroshev-like $D(I)$, **how can we reconstruct $\boldsymbol{D(I)}$?**
- Previous collimator scans operated with the target of reconstructing a local diffusion coefficient, without making assumptions on an amplitude-dependent functional form for $D(I)$;
- **Based on our functional form**, we have proposed an **optimized collimator scans protocol** to enable $D(I)$ reconstruction via the BLM signal.
- The core idea is that BLM signal can be **separated into two distinct processes:** a slow global current $J_{eq}(t)$ and a fast recovery current $J_R(t)$;
- $J_R(t)$ is rich in information about $D(I)$.

A BLM signal composed of two processes

- Assuming a diffusive behavior, with a jaw positioned at I_a, we have that the beam halo will relax to a semi-stationary distribution, which gives us a **global current**:

$$\rho_{eq}(I,t;I_a) = \alpha(t)\int_I^{I_a}\frac{\mathrm{d}x}{D(x)}, \qquad \alpha(t) = \frac{\rho_0\left(I_0(t)\right)}{\int_{I_0(t)}^{I_a}\frac{\mathrm{d}x}{D(x)}} = J_{eq}(t)$$

- When I_a is changed rapidly to a different I_a', the system will relax to a new ρ_{eq}. This gives us a fast **recovery current** $J_R(t) = J(t) - J_{eq}(t)$.

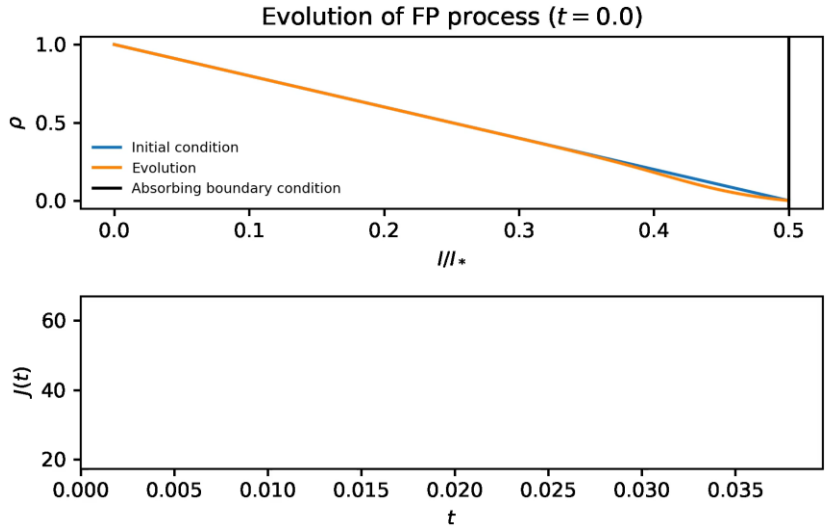

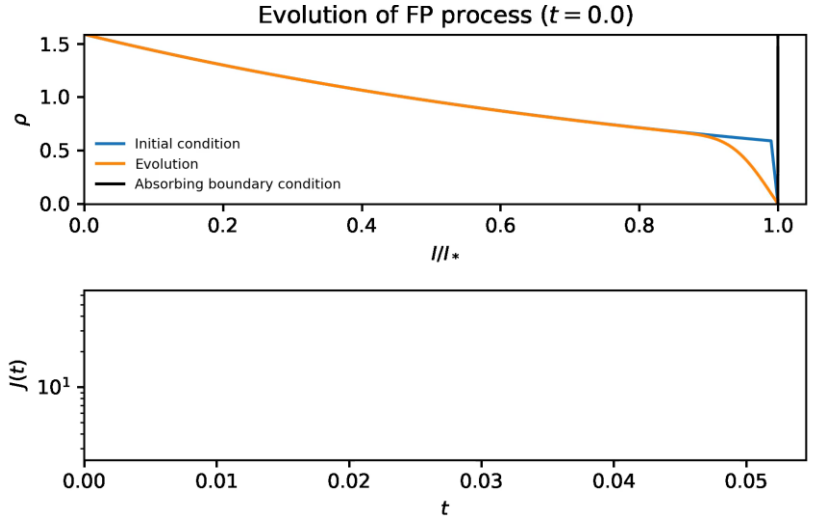

Our measurement protocol proposal

- As the recovery current is rich in information about $D(I)$, we have proposed a repetition of 3-step outward-inward-outward collimator jaw movements;
- **Long pauses between steps** and **data from both inward and outward movements** enables us to reconstruct the global current and fit the recovery current;
- Simulation results tell us that this protocol is best suited when working in the $I/I_* < 1$ domain.

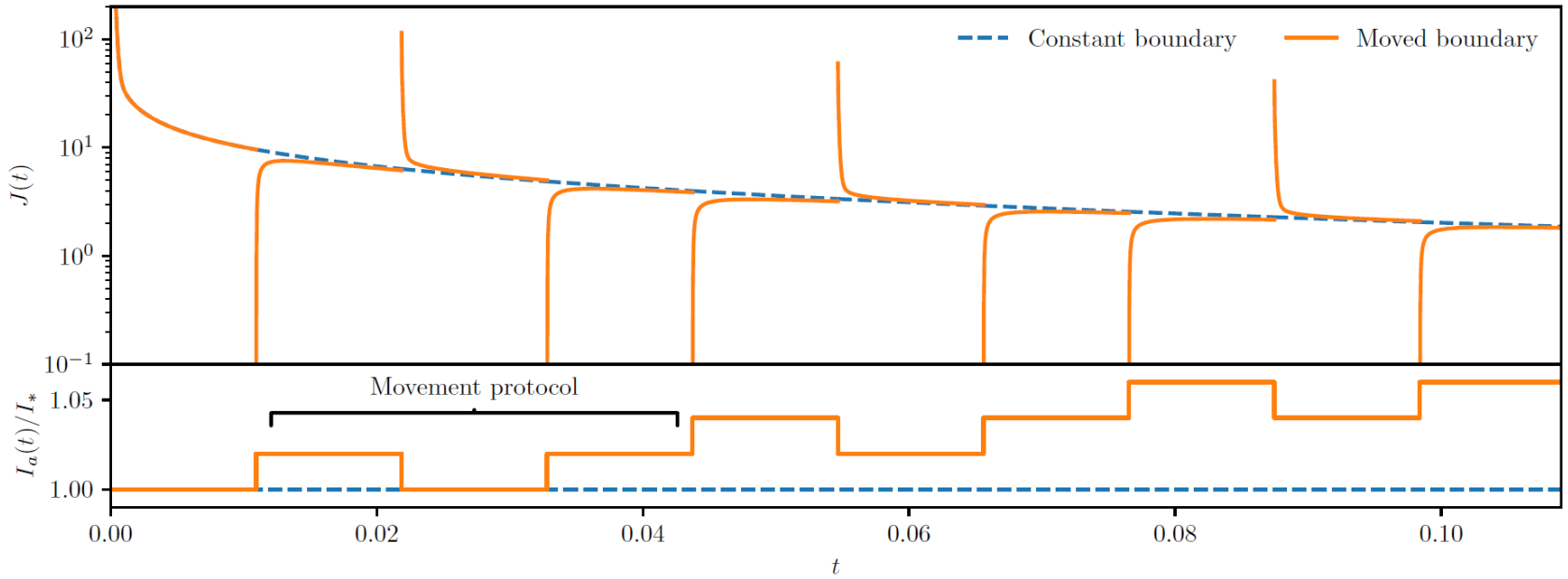

LHC collimator scans from Run 2

- Between 2016 and 2018, collimator scans were performed at the CERN LHC with physics beams at 6.5 TeV;
- Scraping with IR7 TCP was done with inwards and outwards small steps;
- The data have evident diffusion-like features, there are two critical aspects:
  1. No alternation of collimator steps (difficult reconstruction of $J_{eq}(t)$);
  2. Short pauses between steps (most assumptions about $\rho_{eq}(I, t; I_a)$ don't necessarily hold between steps).

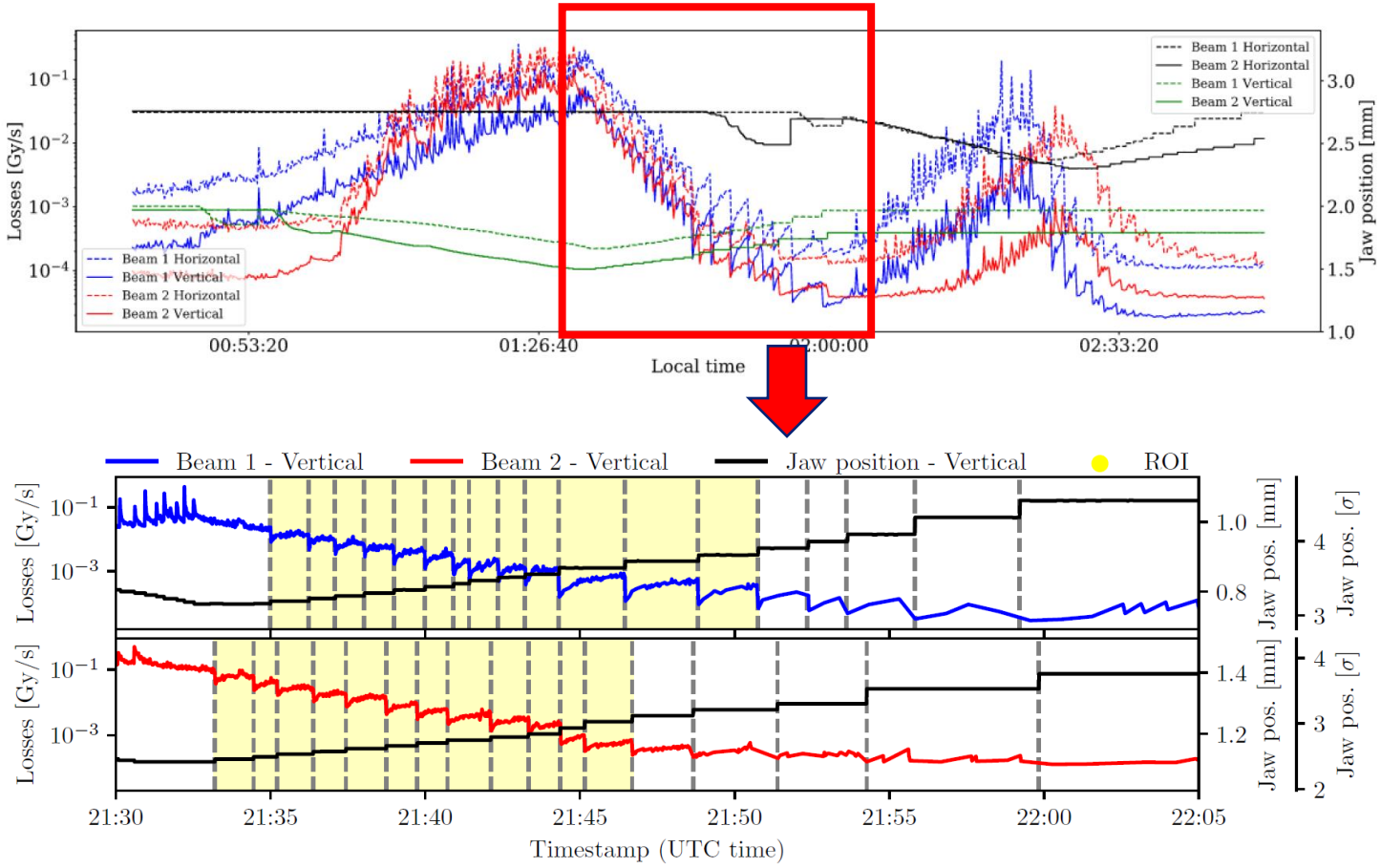

LHC collimator scans from Run 2

- Despite the differences in measurement protocol, we managed to obtain promising results;
- Multiple global current reconstruction and distribution approximations (CSI and M) were tested to reconstruct the lacking information;
- The reconstructed data is then used for the diffusion fit;
- The results were presented at IPAC'22.

Beam / Plane	CSI	M	κ	I_* [σ]
Beam 1 / V	$\times 1.5$	750	0.59 ± 0.03	21 ± 2
Beam 2 / V	$\times 1.5$	1000	0.85 ± 0.02	39 ± 8

Previous work	κ	I_* [σ]
Bazzani et al. [4], Beam 2 / V	0.33	21

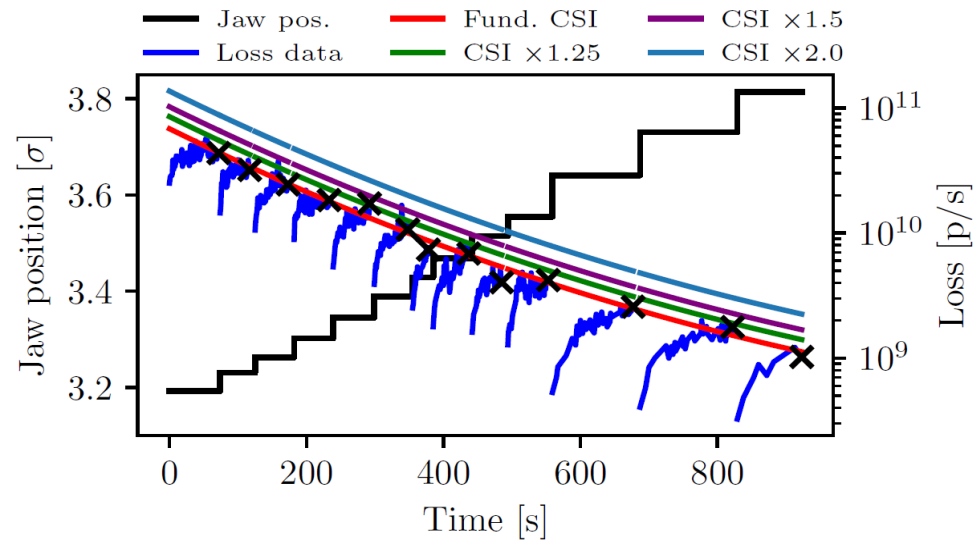

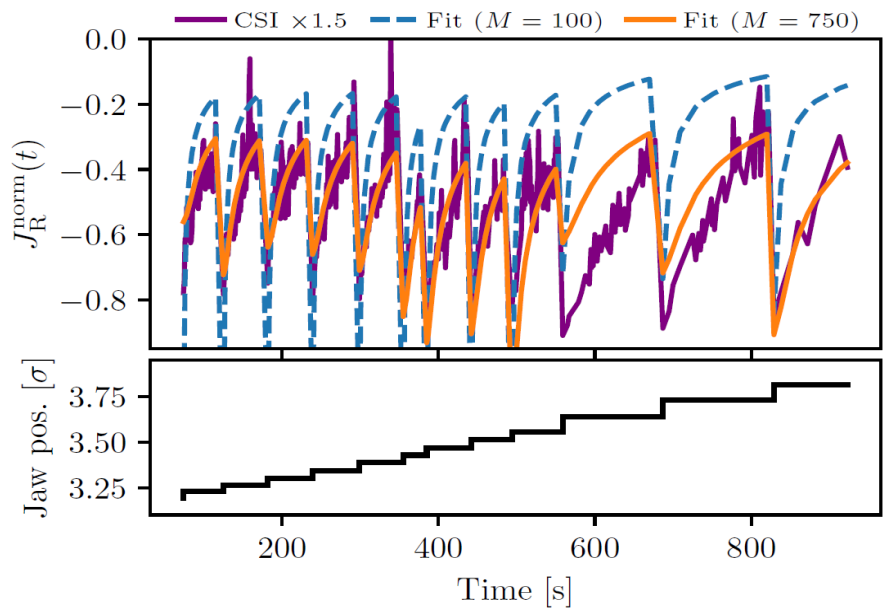

Diffusion model applied to beam-beam wire compensator data

- Beam-beam (BB) wire compensators are DC wires that are used to cancel the effects of long-range beam-beam effects;
- To better understand the effect of BB wire compensators on beam halo, we applied our FP diffusion model to the Run 2 data;
- BLM calibrated losses taken with
  - 4 Different collision angles;
  - Wire compensators on/off on Beam 2;
  - Octupoles @250/-500 A;
  - Beam current transformer data.
- Various chunks of data at different combinations of parameters.

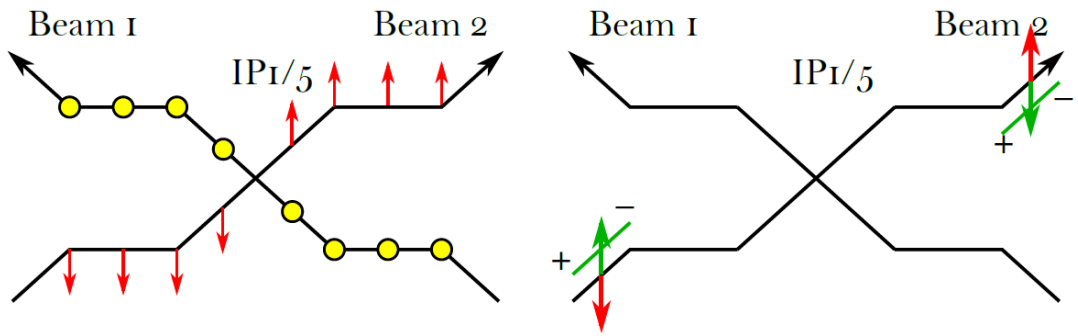

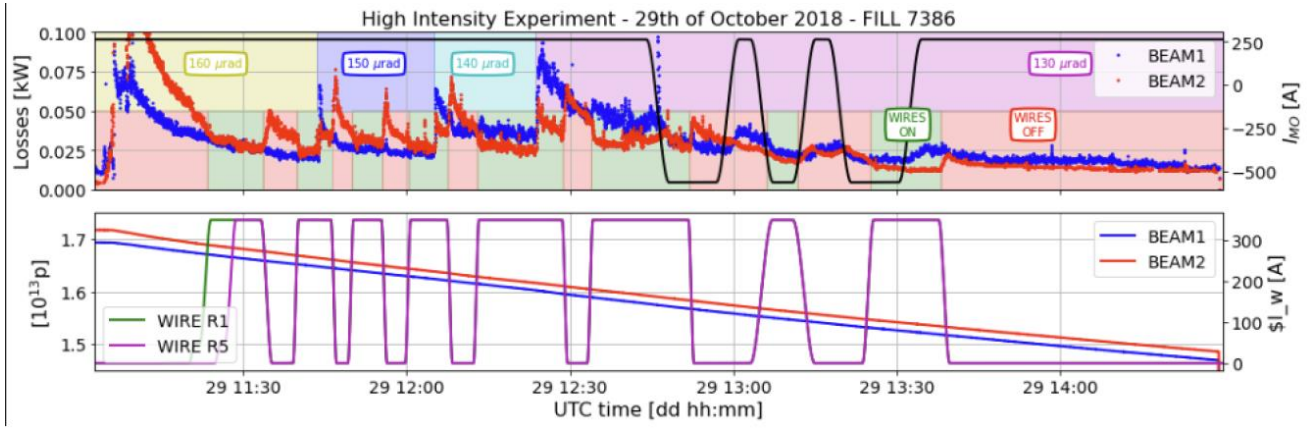

Diffusion applied to BB wire compensator data

- $D(I)$ estimate was obtained by means of a direct fit of a FP process;
- Reconstructed $D(I)$ is in general always lower with Wires ON, suggesting improved losses/emittance values on longer times;
- Preliminary results were presented at a Nonlinear WG; the complete study was presented at IPAC'23.

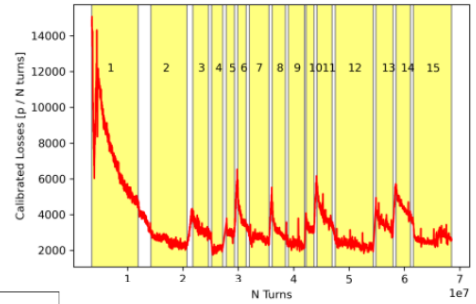

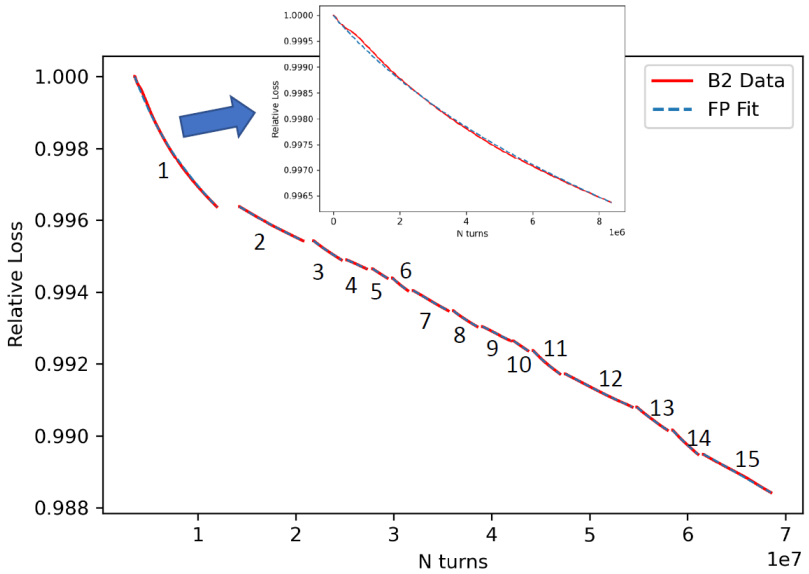

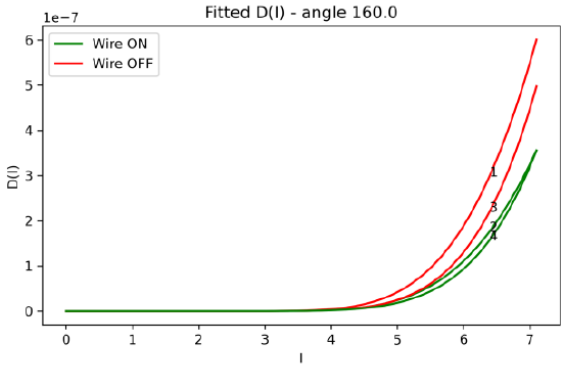

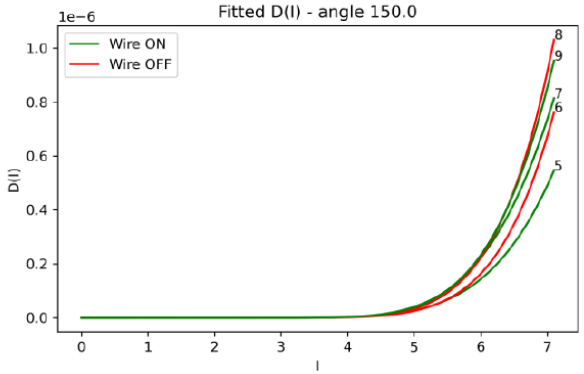

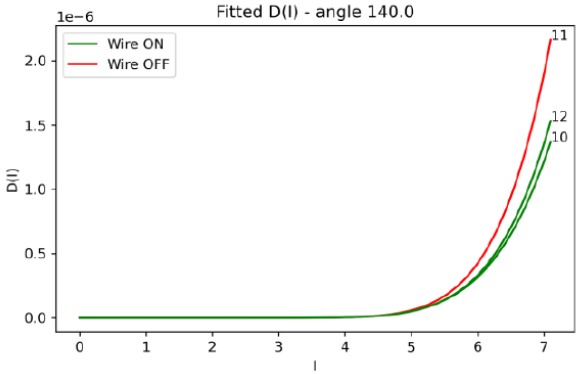

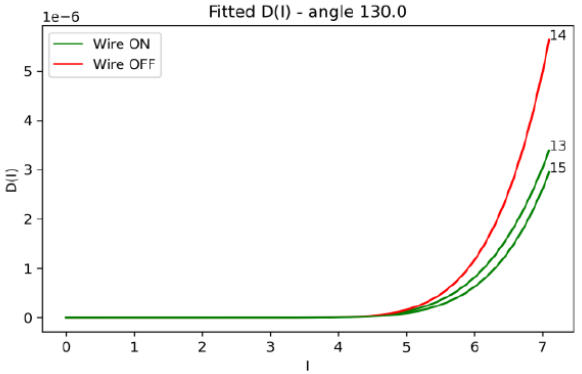

Any recent developments?

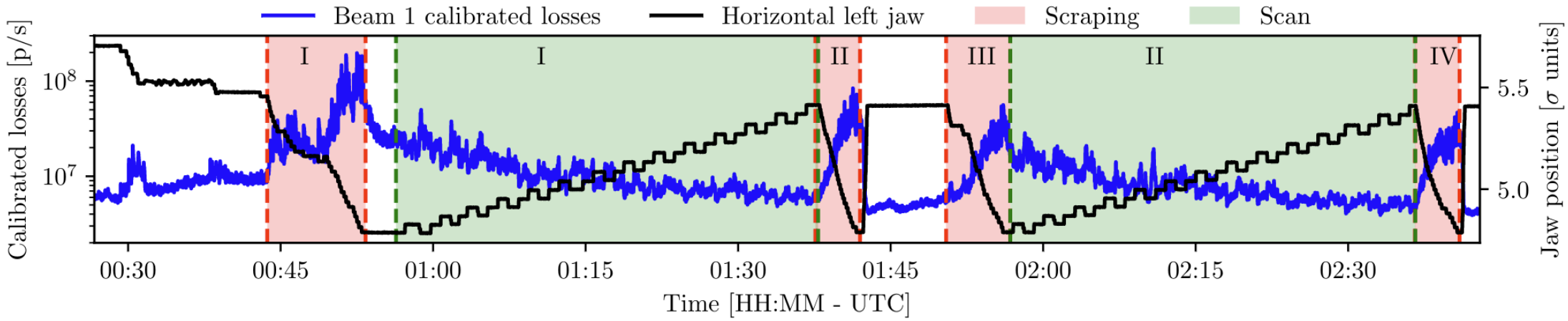

- We had the possibility to execute the scraping during LHC Run3:
  - On 600b and 1200b «End of Fill», with separated beams;
  - At the end of a dedicated BB wire compensator measurement, with both wires on and off;
- These first opportunities, especially the last one, will give us insights on how different configurations can affect both the diffusion and the performance of our protocol.
- Some first fit results (not included in the thesis) were presented at IPAC'23.

Chaos indicators for single-particle tracking

Chaotic regions and diffusion

- Diffusion-like behavior are **related** to the existence to **weakly chaotic regions** in the phase space;
- The existence of these regions is described by the KAM and Nekhoroshev theorems;
- We are interested in exploring tools to **detect and quantify** these regions in **tracking simulations**;
- By using **chaos indicators** in single-particle tracking, we hope to better inspect and evaluate the regularity of accelerator lattices.

Dynamic indicators – quick overview

Within the accelerator physics community, two well-known tools in the sector of indicators of chaos are:

- **The Fast Lyapunov Indicator** (FLI), a direct evaluation of the Maximal Lyapunov Exponent on a finite number of turns (implemented in Sixtrack by means of pair particles);
  - A numerical estimate of $\boldsymbol{\Xi}_n(\boldsymbol{x})$ is evaluated on a finite n;
  - FLI/n converges to zero if the orbit is regular;
  - FLI/n eventually saturates to the value of the Maximal Lyapunov Indicator for a chaotic orbit;

- **The Frequency Map Analysis (FMA),** which evaluates the variation of the tune of an initial condition over different time intervals
  - A regular initial condition must have the same tune over long time intervals;
  - A chaotic initial condition, conversely, will not have a tune;

Dynamic indicators – quick overview

In our recent study, we investigated the performance of less-known dynamic indicators, such as:

- **Fast Lyapunov Indicator with Birkhoff weights (FLI^{WB});**
  - An "enhanced" FLI which makes use of the superconvergence properties provided by the Birkhoff weights to achieve convergence rates faster than FLI
- **Reverse Error Method (REM);** Uses the numerical uncertainty as a tool to evaluate the orbit chaotic behaviour. By performing a tracking and backtracking of n iterations, we can use the resulting displacement from the original initial condition as a measure of chaos.
  - A regular orbit will have a displacement following a power law.
  - A chaotic orbit will instead exhibit an exponential increase, given by the Maximal Lyapunov Exponent

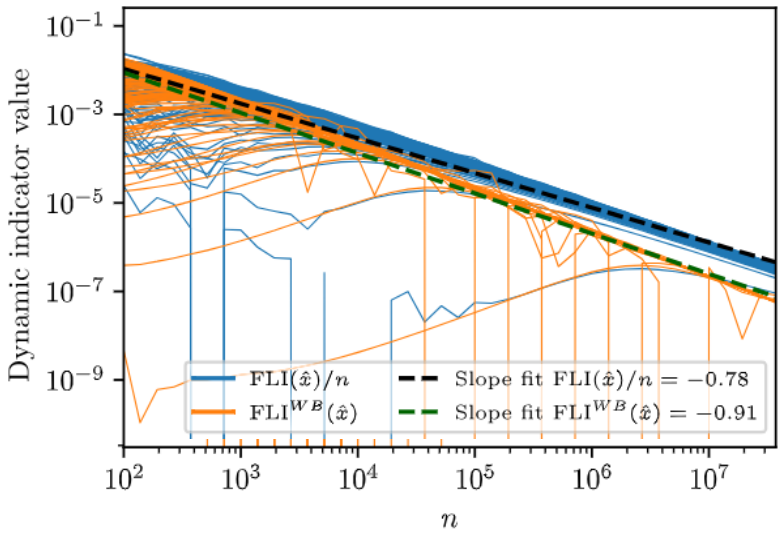

Convergence comparison of regular particles in a Modulated Hénon Map. FLI^{WB} converges faster than FLI/n to zero. (source)

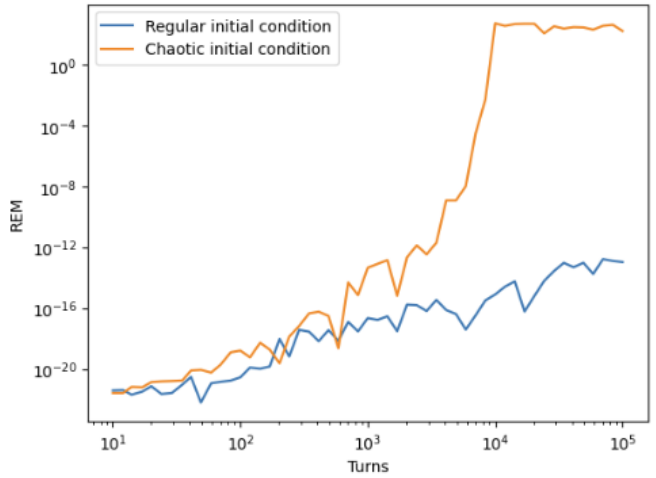

Comparison between regular and chaotic REM. Chaotic REM exponentially increases up to a saturation value corresponding to the «diameter» of the explorable phase space.

Dynamic indicators – quick overview

- **Generalized Alignment Index ($GALI$);**
  $GALI^k$ considers the evolution of $\boldsymbol{k}$ initial orthonormal displacements, then, evaluates the volume of the parallelotope whose sides are the normalised images of the evolved displacements.
  - For a **chaotic orbit**, these displacements will eventually **align exponentially fast** towards the autovector of the maximal Lyapunov exponent (i.e., **volume zero**);
  - For a **regular orbit**, the volume of the parallelotope **either stays constant or decreases following a power law** depending on $\boldsymbol{k}$.

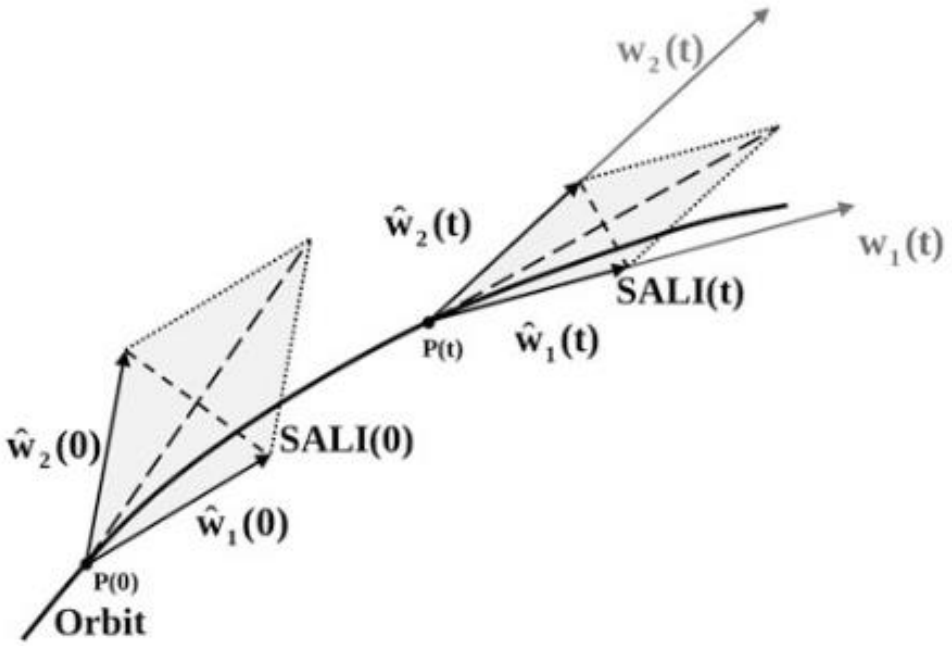

Schetch of the Smallest Alignment Index ($SALI$) indicator, which is mathematically equivalent to $GALI^2$. (source)
The displacements along the chaotic orbit progressively align over the Maximal Lyapunov Exponent.

Dynamic indicators – quick overview

- **Lyapunov Error** (LE); instead of estimating the linear response of the system on a single displacement like FLI, it considers the trace of the covariance matrix of the full **tangent map** $\mathrm{L}_n(\boldsymbol{x}) = DM(\boldsymbol{x}_{n-1}; n-1) \dots DM(\boldsymbol{x}_0; 0)$, that is

$$LE_n(\boldsymbol{x}) = \sqrt{\mathrm{Tr}(\mathrm{L}_n^T(\boldsymbol{x})\mathrm{L}_n(\boldsymbol{x}))}.$$

- **Mean Exponential Growth of Nearby Orbits** $(MEGNO)$;
  - Reduces the fluctuations of a "direct" evaluation of an indicator such as FLI or LE by means of a **double-time average filter**.
  - The resulting indicator reads (for the case of LE):

$$MEGNO_n\big(LE(\boldsymbol{x})\big) = \left\langle\left\langle t\,\frac{d\log LE_n(\boldsymbol{x})}{dt}\right\rangle\right\rangle \quad \text{where} \quad \langle f(t)\rangle = \frac{1}{t}\int_0^t f(t')dt$$

Dynamic indicators on the modulated Hénon map

- 4d polynomial time-dependent symplectic map;
- Straightforward implementation on GPU architectures, possible to reach high iteration times ($n = 10^8$)

$$\begin{pmatrix} x_{n+1} \\ p_{x,n+1} \\ y_{n+1} \\ p_{y,n+1} \end{pmatrix} = R(\omega_{x,n}, \omega_{y,n}) \times \begin{pmatrix} x_n \\ p_{x,n} + x_n^2 - y_n^2 + \mu\left(x_n^3 - 3x_n y_n^3\right) \\ y_n \\ p_{y,n} - 2x_n y_n + \mu\left(y_n^3 - 3y_n x_n^3\right) \end{pmatrix}$$

$$\omega_{x,n} = \omega_{x,0}\left(1 + \varepsilon \sum_{k=1}^{m} \varepsilon_k \cos\left(\Omega_k n\right)\right)$$

$$\omega_{y,n} = \omega_{y,0}\left(1 + \varepsilon \sum_{k=1}^{m} \varepsilon_k \cos\left(\Omega_k n\right)\right)$$

k	Ω_k	$10^4 \epsilon_k$
1	$2\pi/868.12$	1.000
2	$2\Omega_1$	0.218
3	$3\Omega_1$	0.708
4	$6\Omega_1$	0.254
5	$7\Omega_1$	0.100
6	$10\Omega_1$	0.078
7	$12\Omega_1$	0.218

$(\omega_{x0}, \omega_{y0}) = (0.28,\ 0.31),\ \varepsilon = 32.0,\ \mu = 0.0, n = 10^5$

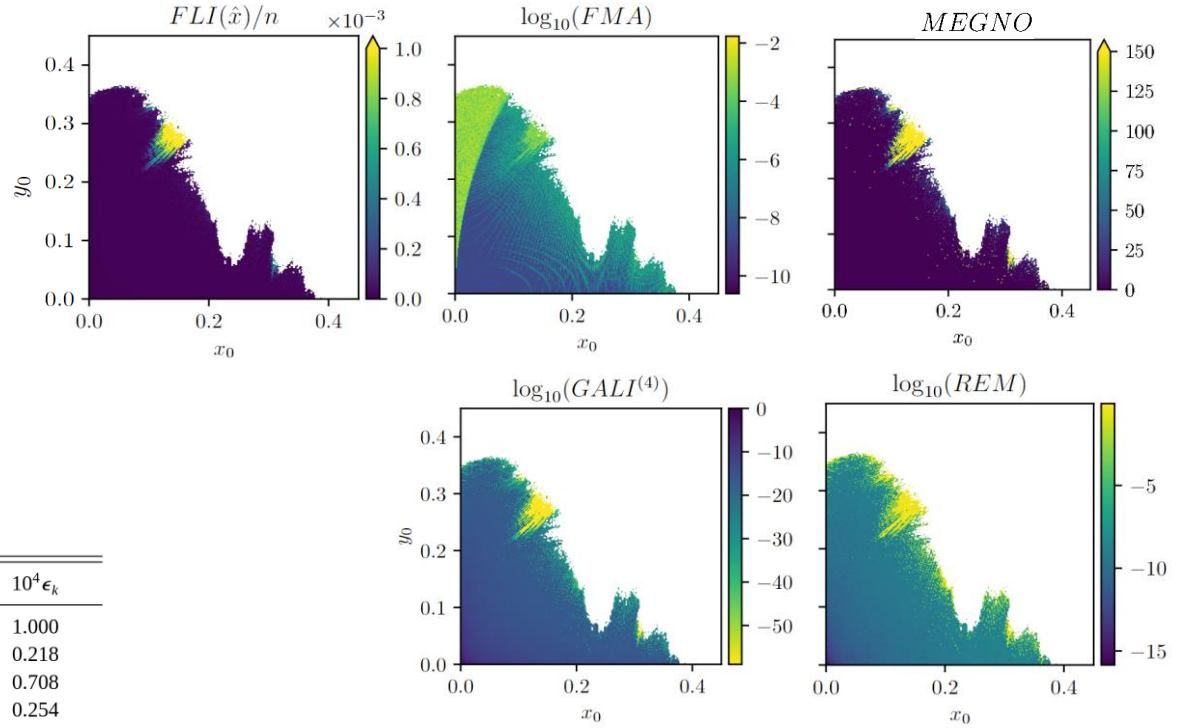

Convergence of dynamic indicators over time

- Dynamic indicators have the tendency to create a **bimodal distribution** over time (with the exception of FMA, which tends to a tri-modal distribution)
  - One populated cluster of regular initial conditions;
  - A minor cluster or spread of values given by the chaotic initial conditions;
- With this setup, we can classify the accuracy of the indicators in reconstructing a Ground Truth evaluated after 10^8 turns.

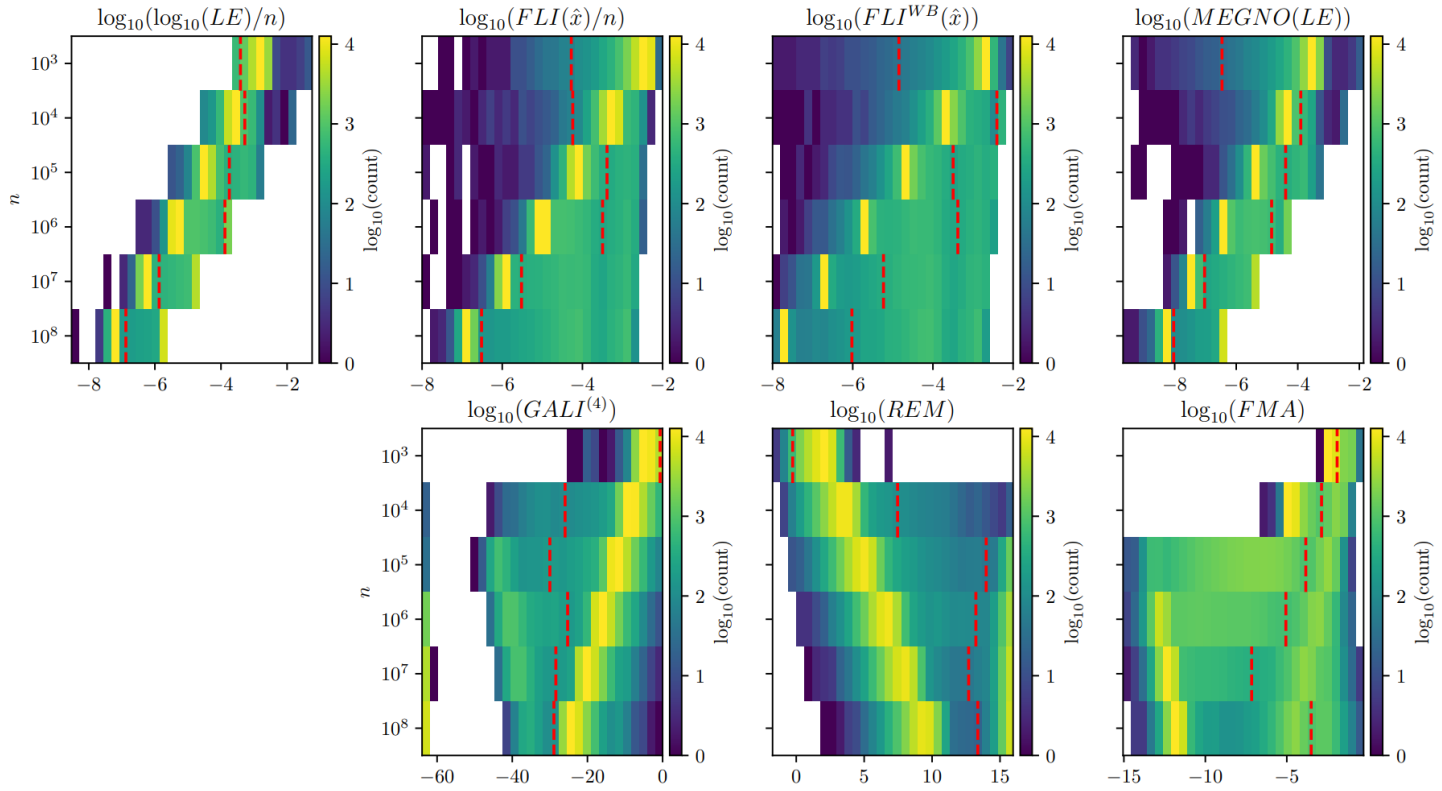

Value distribution over time of dynamic indicators on a Hénon map
Simulation parameters: $(\omega_{x0}, \omega_{y0}) = (0.28, 0.31), \varepsilon = 32.0, \mu = 0.5$

Defining the classification performance

- "Agnostic" thresholding algorithm for detecting the two main distribution modes;
  - Returns a binary classification threshold regular/chaotic;
- Kernel Density Estimate (KDE) with progressively smaller bandwidth
  - Bandwidth reduction stops when the fluctuations in the distributions become significant;
- For the specific case of FMA, the algorithm looks for three modes.

Overview of KDE based thresholding algorithm for REM (top) and FMA (bottom)

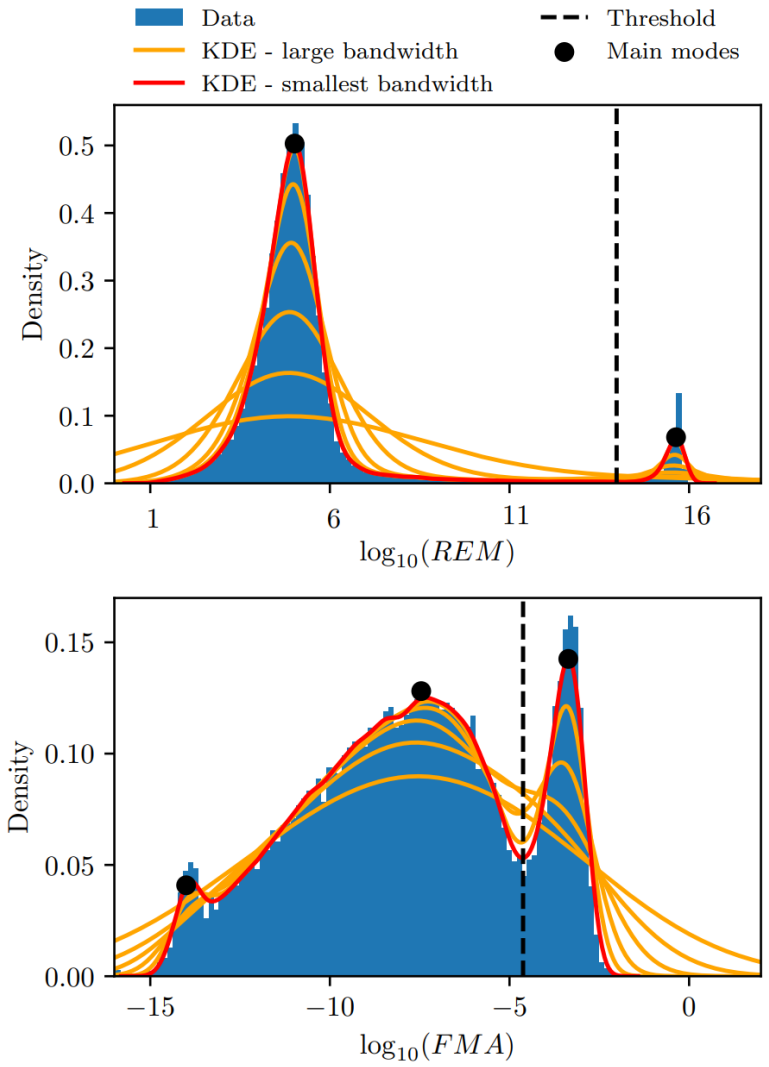

Defining a Ground Truth (GT)

- From the algorithm, we define a Ground Truth (GT) using the $\log_{10}(\log_{10}(LE)/n)$ value with $n = 10^8$;
- Well defined distinction between chaotic and regular initial conditions;
- A good-performing indicator will reconstruct the GT at lower n values. Conversely, a bad-performing indicator will require higher n values.

Visualization of GT construction

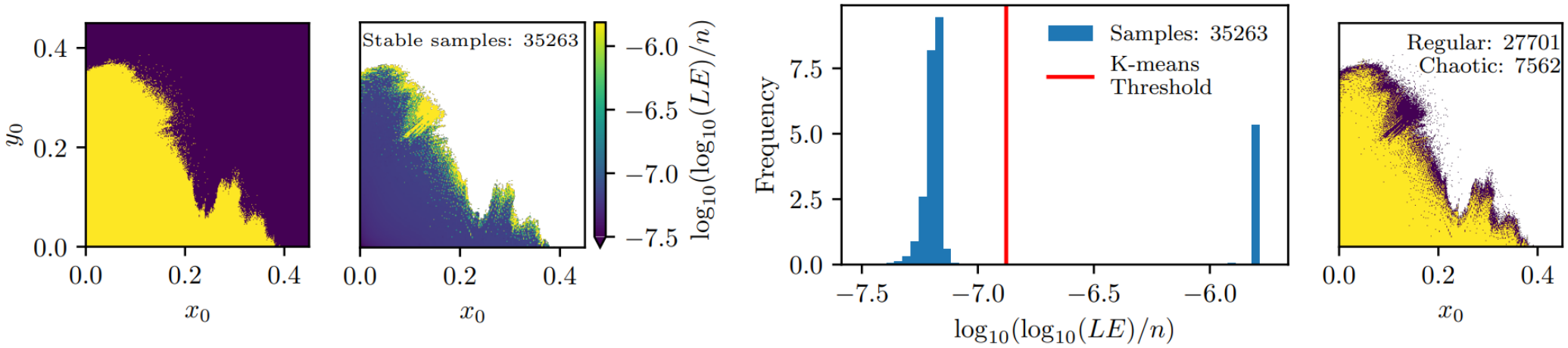

Final considerations from the Hénon map

From the analysis of the Hénon map, we have learned the following things:

- $\boldsymbol{REM}$ **and** $\boldsymbol{GALI^{(k)}}$ indicators seem to provide the **best performance** in fast detection of chaos;
- **Superconvergence** by means of **Birkhoff weights** can be used for evaluating FLI, namely, FLI^{WB}. Therefore, it's a preferable method for estimating the maximal Lyapunov exponent.
- If we are interested in chaos detection only, $\boldsymbol{FMA}$ **might be affected by resonance lines and modulation effects.**

This knowledge can be **transported** to more realistic accelerator lattices.

Accuracy evolution over time for the various dynamic indicators

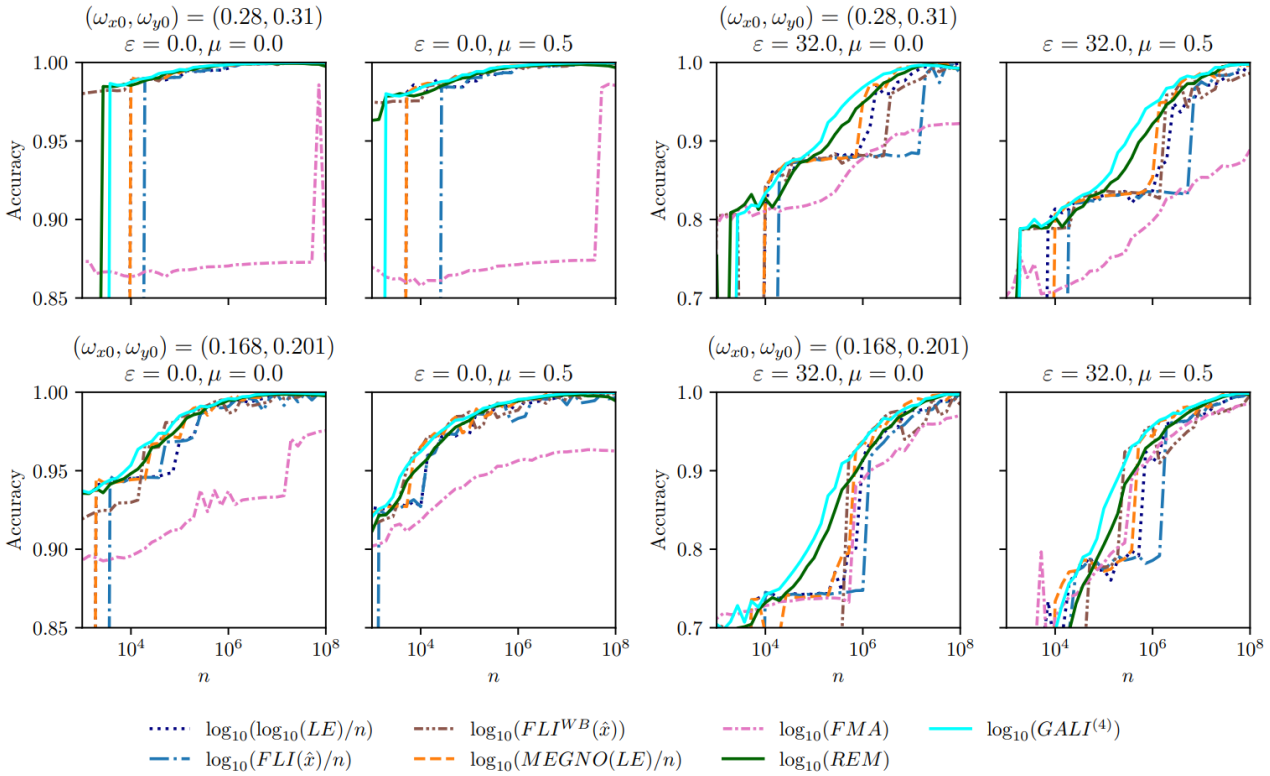

Application to a realistic HL-LHC lattice

HL-LHC characteristics

- HL-LHC v1.4 Beam 1 optics;
- Colliding beams at top energy;
- No beam-beam interactions;
- Two different magnet noise realisations
  - Out of the table of 60 seeds, we picked the ones which scored, respectively, the best and worst Dynamic Aperture at $n = 10^5$ turns.
- Three different values of ζ_0
  - Reference orbit, half of the bucket, near the bucket separatrix.

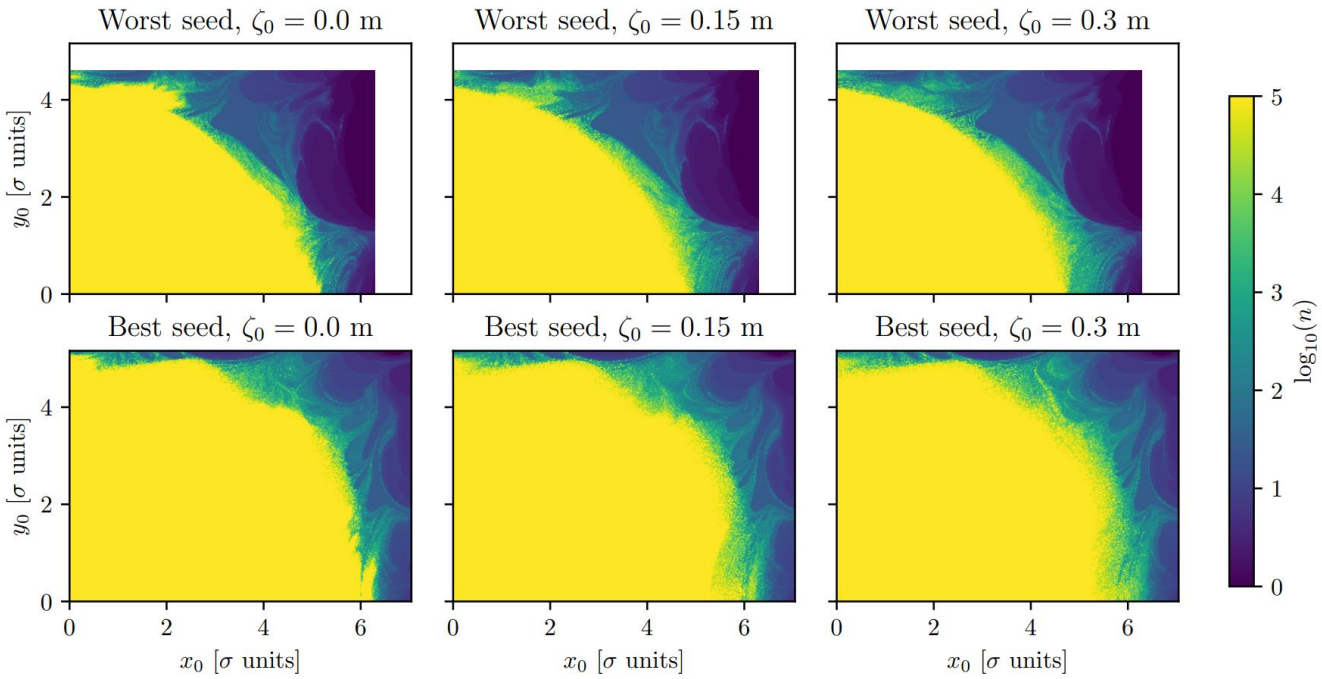

Survival plot of HL-LHC ($n_{\max} = 10^5$)

Evaluating chaos indicators without a tangent map expression

- Current tools do not offer analytical expressions of the tangent map of realistic lattices;
- To overcome this issue, we implemented the "shadow particle" method to numerically estimate it for a given displacement $\epsilon\boldsymbol{\xi}$:
  - Given an initial condition $\boldsymbol{x}_0$ to track, also track $\boldsymbol{y}_0 = \boldsymbol{x}_0 + \epsilon\boldsymbol{\xi}$.
  - Every τ turns, renormalize the distance between $\boldsymbol{y}$ and $\boldsymbol{x}$ to ϵ.
- Straightforward implementation for evaluating both linear response and evolution of the displacement direction over time.

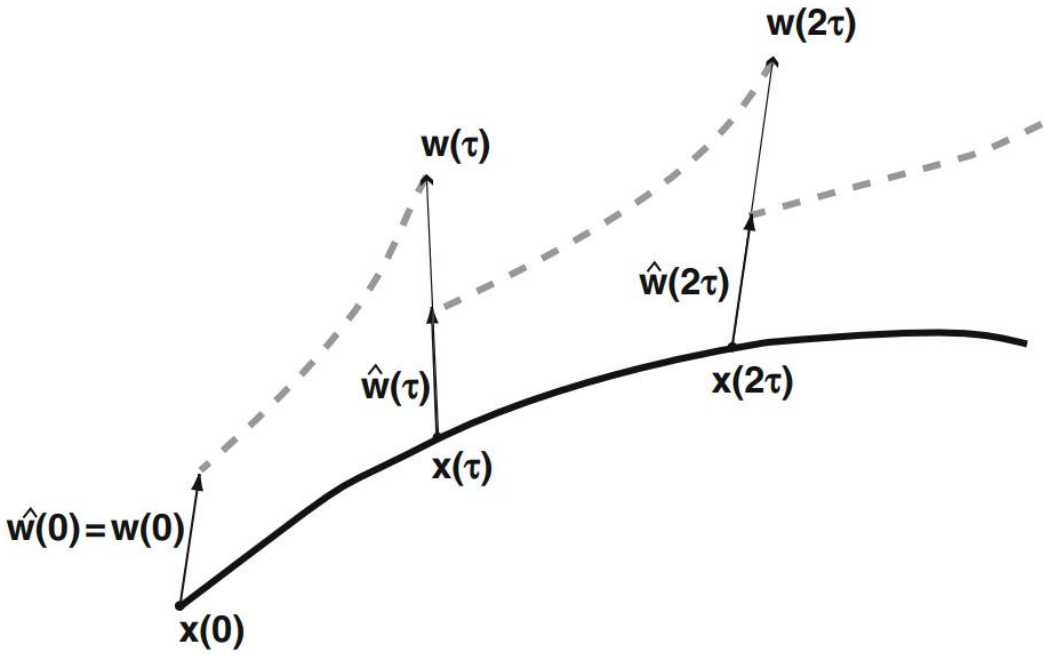

Sketch of the ghost particle method

Implementation on Xsuite

- Simulation of an HL-LHC realistic lattice via the new software Xsuite;
- Straightforward GPU single-particle tracking implementation;
- Easy to implement “custom” normalisation of ghost particles;
- GPUs enable scale-up of initial conditions and consequent statistical analysis;
  - Tracking 10^5 particles up to 10^5 turns takes ~2.5h on a Nvidia Tesla A100;
- We inspected FLI/n, FLI^{WB}, REM, $GALI^{(k)}$, and FMA.

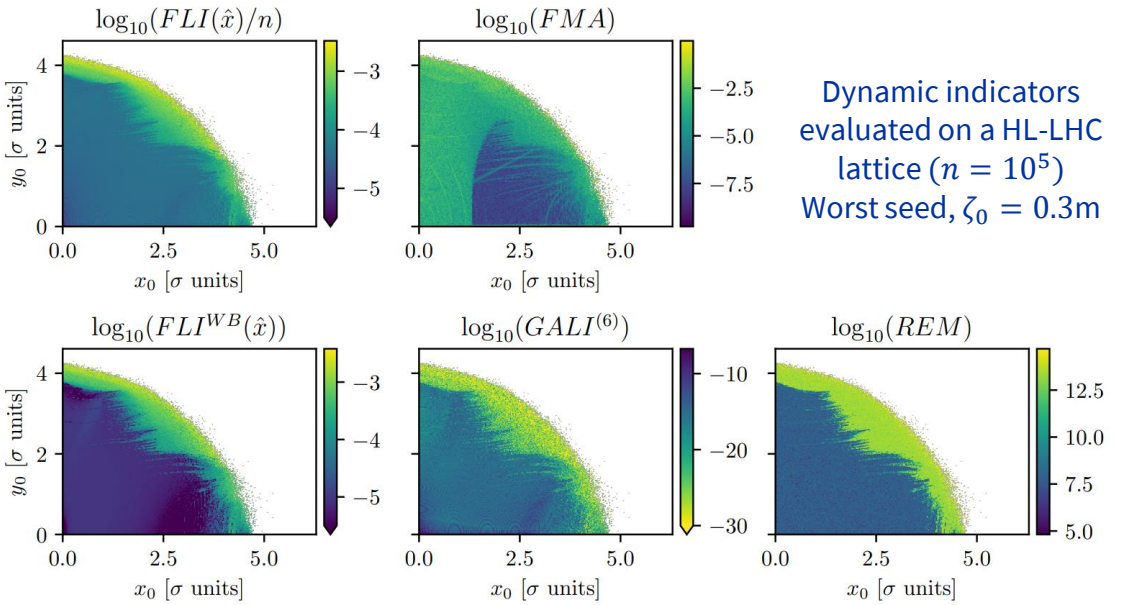

Dynamic indicators evaluated on a HL-LHC lattice ($n = 10^5$)
Worst seed, $\zeta_0 = 0.3$m

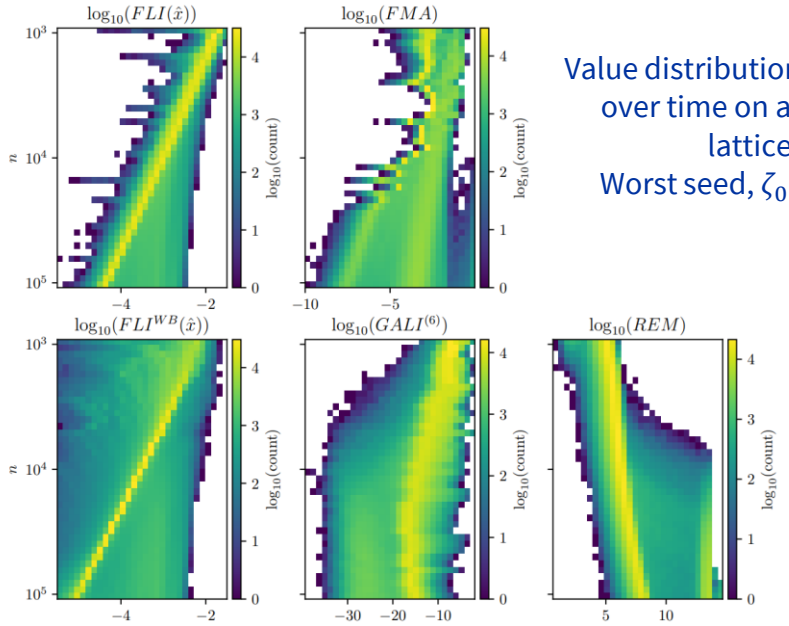

Value distribution evolution over time on a HL-LHC lattice
Worst seed, $\zeta_0 = 0.3$m

Inspecting the Lyapunov Time

- The **Lyapunov Time T_L** is defined as the **inverse** of the Maximal Lyapunov Exponent λ_1^{-1} and represents the "timescale" of the chaotic behaviour (as the linear response is $\approx e^{\lambda_1 n}$);
- It is **not possible** to draw a universal one-to-one relation between the stability time T_S of a particle and its T_L:
  - Cases of stable chaos and resonance-related instabilities make such connections impossible to draw;
- However, studies in astrophysics (e.g., Morbidelli et al.) investigated the possible correlation laws between the stability time T_S and T_L;
- These lines of research might suggest interesting path in **statistical investigations and scale-law-based extrapolations:**
  - A standard statistical investigation consists in inspecting the mean T_L and T_S value at different amplitudes.

Evaluation on a realistic HL-LHC lattice
(More on that in the next slides!)

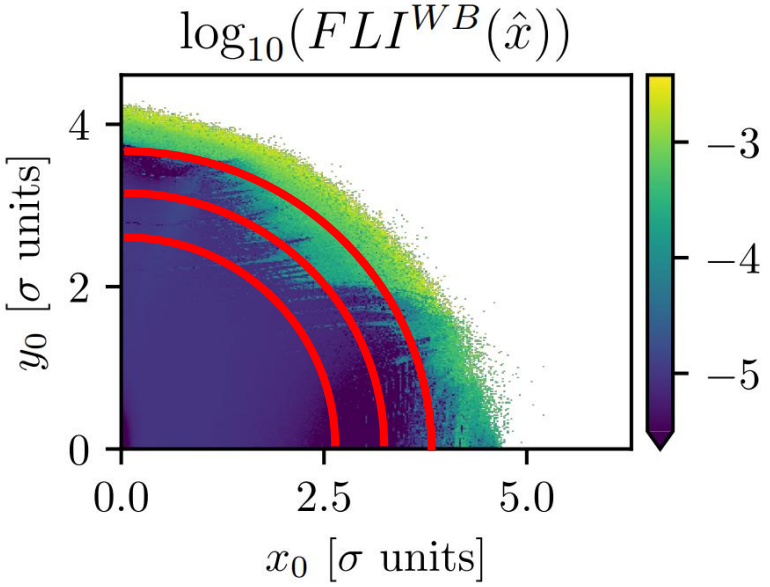

Sketch of different amplitudes over which the mean value is measured

Correlations and scale laws for T_S and T_L

- From well-established Dynamic Aperture scale laws, we expect T_S to follow a Nekhoroshev-like scale law

$$T = T_0 \exp\left[-\left(\frac{I_*}{I_0}\right)^{\frac{1}{2\kappa}}\right]$$

- The Nekhoroshev character of a system is related to the breaking of the regular KAM tori geometry due to the presence of high-order resonances and non-linear contributions;
- Relation expected with the presence of macroscopic chaotic regions in the phase space;
- We expect to observe a similar Nekhoroshev-like scale law on T_L as well!
- This would also imply the existence of a correlation law between T_S and T_L
  - Many proposals exist in literature, e.g., $T_L = \alpha T_S^{\beta}$

Radial mean of T_L and T_S. T_S evaluated @ 10^6 turns. T_L evaluated @ 10^5 turns

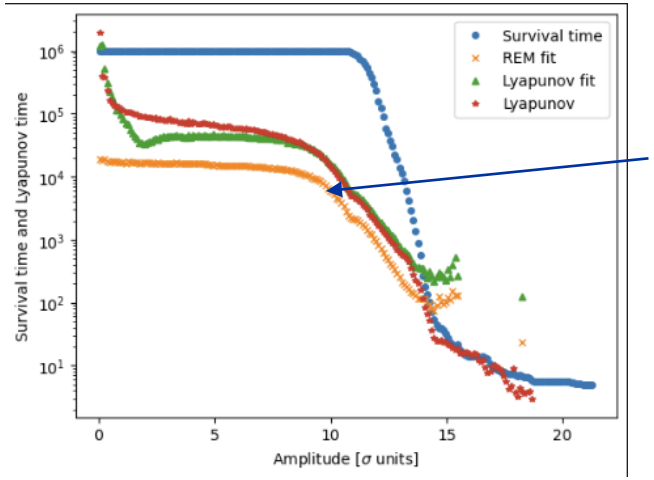

«deeper» information with less turns? Maybe!

Testing a functional law for correlation presented in literature (source)

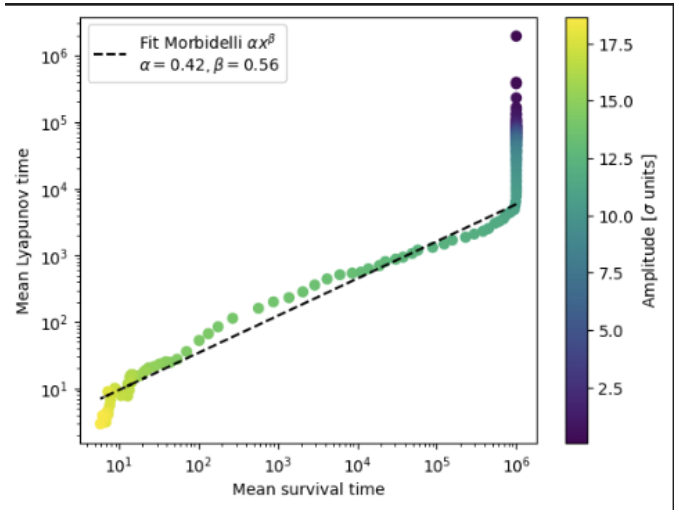

To summarize

- Proposal for optimized collimator scans protocol;
- Application of the diffusive framework on Run 2 collimator scans and wire compensators data;
- Initial End of Fill measurements in Run 3;
- Diffusion measurements performed at the end of the last wire compensators measurements;
- Implementation and analysis of dynamic indicators for probing the chaotic behavior in particle tracking for realistic accelerator lattices.

Thank you!

Link to the thesis:

Publications

- (In preparation) R. Appleby, A. Bazzani, A. Fornara, M. Giovannozzi, C.E. Montanari, G. Sterbini, G. Turchetti. *"Chaos indicators and nonlinear dynamics in circular particle accelerators"*.
- A. Bazzani, M. Giovannozzi, C.E. Montanari, G. Turchetti. *"Performance analysis of indicators of chaos for nonlinear dynamical systems"*. Phys. Rev. E 107, 064209 (2023).
- C.E. Montanari, A. Bazzani, M. Giovannozzi. *"Probing the diffusive behaviour of beam-halo dynamics in circular accelerators"*. Eur. Phys. J. Plus (2022).
- M. Giovannozzi, E.H. Maclean, C.E. Montanari, G. Valentino, F.F. Van der Veken. *"Machine Learning Applied to the Analysis of Nonlinear Beam Dynamics Simulations for the CERN Large Hadron Collider and Its Luminosity Upgrade"*. Information, 12(2), 53 – 2020.
- Bazzani, A., Giovannozzi, M., Maclean, E. H., Montanari, C. E., Van der Veken, F. F., and Van Goethem, W. *"Advances on the modeling of the time evolution of dynamic aperture of hadron circular accelerators"*. Phys. Rev. Acc. and Beams, 22(10), 104003.

carlo.emilio.montanari@cern.ch

Backup slides

Recent Run3 Data

Run 3 loss data

- Collimator scan performed at the end of wire-compensator MD (MD8043)

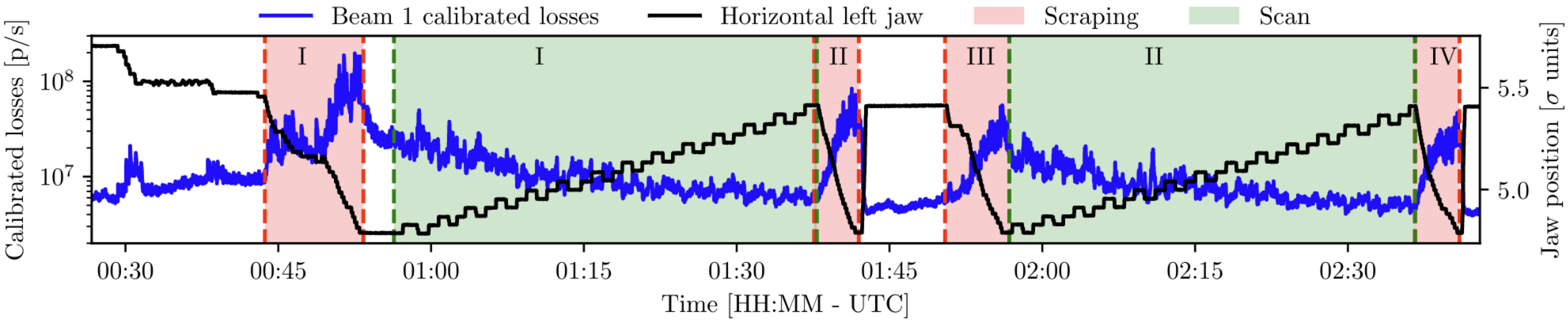

- Two collimator scans on the horizontal plane of Beam 1 (measured sigma units are reported);
- Scraping performed before and after the scans;
- First scraping performed after ~6 hours of beam operation and a beam-based alignment.

First estimate of beam tail distribution

- We construct an initial estimate of the beam tail population using the collimator scraping data;
- The integrated losses measured during each collimator step are taken as an estimate of the proton population in that specific segment;
- The first reconstruction differs from the other three (time passed before the scraping is different);
- Following the double-gaussian model, a Gaussian fit is used as first estimate of the beam tail population;
- We consider the first reconstruction as a $\rho_0(I)$ estimate.

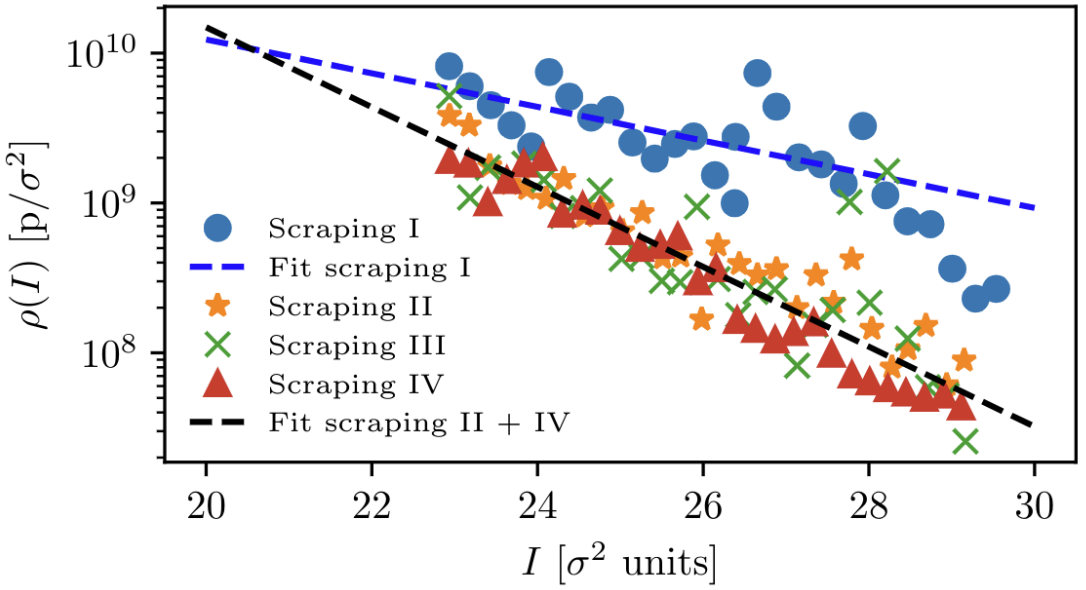

Inspecting J_{eq} at different I_a

- With the collimator scan movement and the time spent between steps, we can assume that the last seconds of loss signal before the next collimator movement is J_{eq} at a specific I_a;
- We consider as measure the mean of the last 10 seconds of signal, and as uncertainty the standard deviation observed;
- The three-step protocol gives us three J_{eq} samplings for various I_a values;
- We assume $I_0(t = t_0)$ for the duration of the scan. However, the second collimator scan does show that I_0 has evolved over the span of ~1 hour, as J_{eq} is lower.

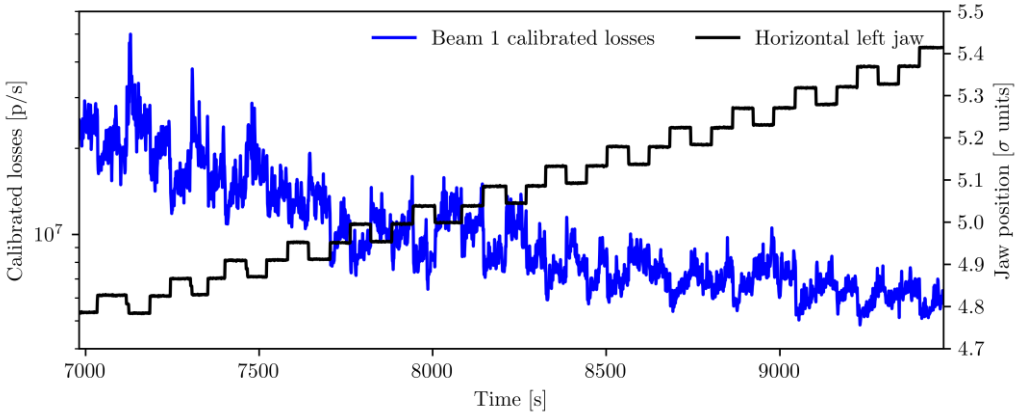

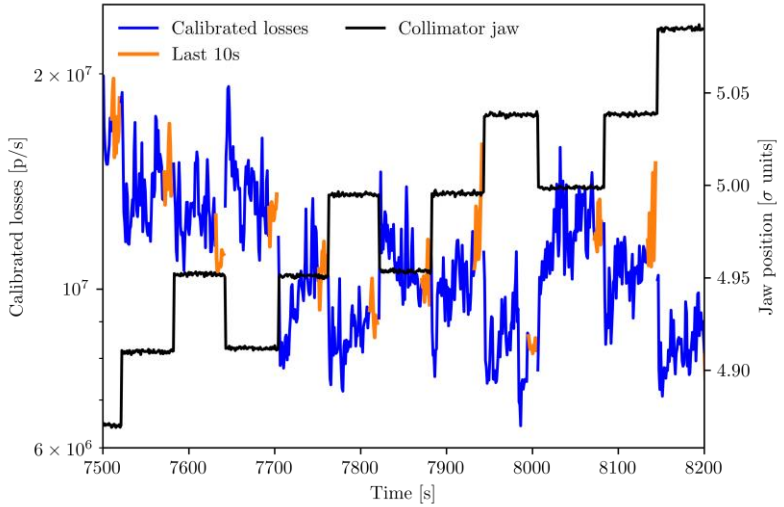

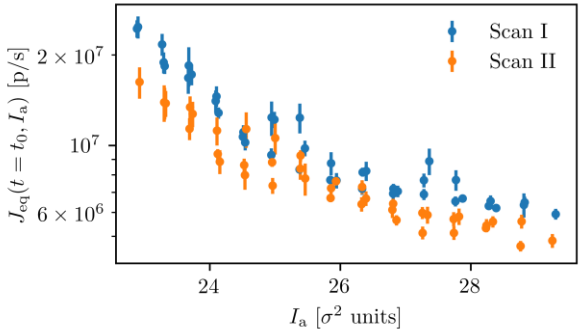

Fitting $D(I)$ using J_{eq} data

- We reconstruct $D(I)$ by means of

$$J_{eq}(t = t_0; I_a) = \frac{\rho_0\big(I_0(t = t_0)\big)}{\int_{I_0(t=t_0)}^{I_a} \frac{\mathrm{d}x}{D(x)}}$$

- While assuming the following:
  - I_* and κ are equal for the two scans (as there is no major variation in the accelerator environment);
  - I_0 can be considered constant for the duration of an individual scan;
  - ρ_0 is given by the gaussian fit of the first beam tail reconstruction.
- This gives us the following free parameters for the fit:
  - I_* and κ, in common for the two scans;
  - $I_{0,\mathrm{I}}$ and $I_{0,\mathrm{II}}$, which are respectively the value of I_0 for the first and second collimator scan.

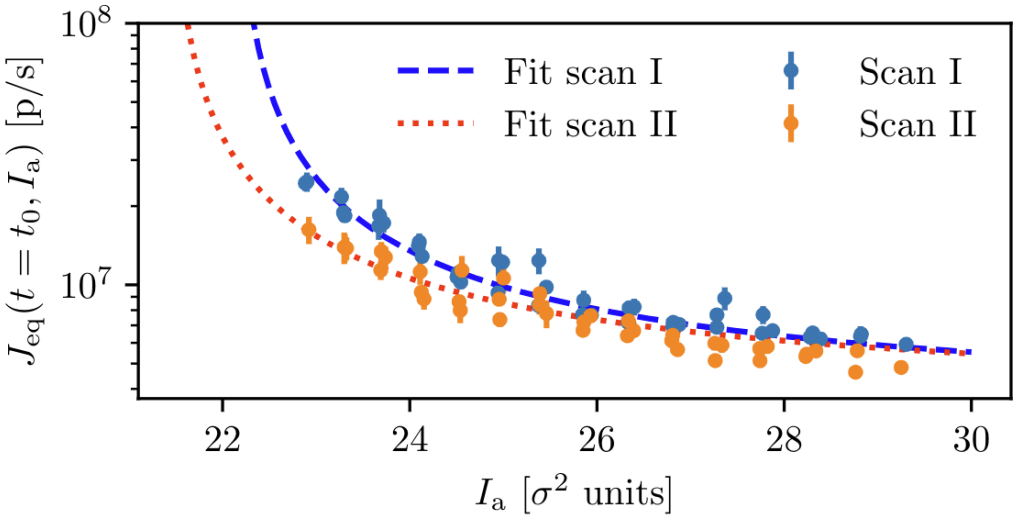

$I_{0,\mathrm{I}}$	$I_{0,\mathrm{II}}$	κ	I_*
22.13 ± 0.06	21.4 ± 0.1	0.47 ± 0.01	61.5 ± 0.2

Constructing $\rho_{\mathrm{eq}}(I)$ using the fitted $D(I)$ parameters

- The reconstructed $D(I)$ can then be used to estimate the initial shape of $\rho_{\mathrm{eq}}(I)$ (although, an initial estimate for $\rho_0\big(I_0(t)\big)$ is still necessary);
- The resulting $\rho_{\mathrm{eq}}(I)$, if compared with the initial Gaussian fit, captures more features of the data;
- This constitutes a nice initial "consistency check" for the diffusive framework.

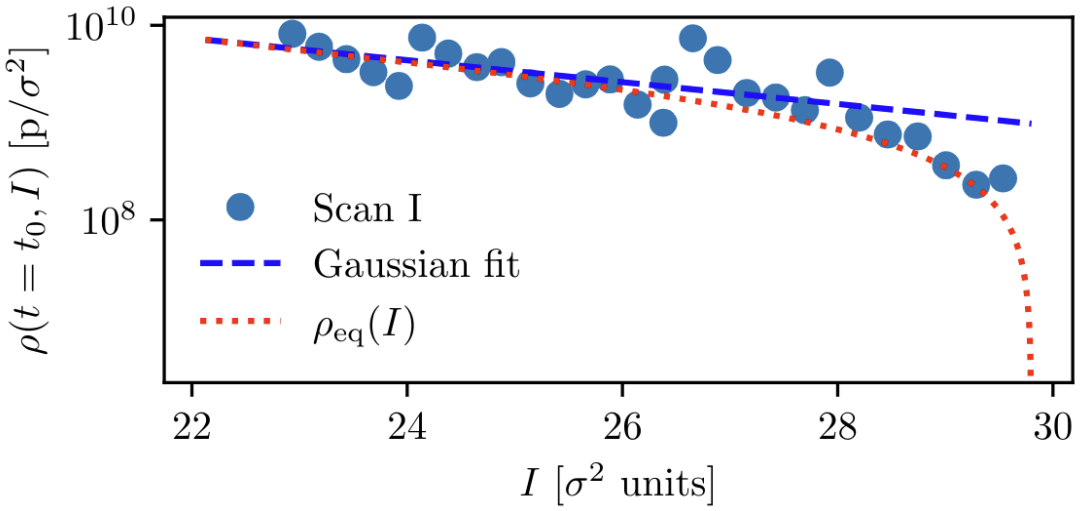

Summary

- The collimator scans performed last year followed the proposed three-step protocol, offering an ideal ground for applying the diffusive framework;
- In this first analysis, we reconstructed a Nekhoroshev-like $D(I)$ by inspecting the J_{eq} value at different collimator jaw positions.

Future work

- Inspection of Beam 2 data, influenced by wire compensators;
- Inspection of recovery currents as cross-check of the reconstructed $D(I)$;
- Inspection of beam tail re-population times by means of our Fokker-Plank models;

Backup slides

More details on indicators of chaos and their application

Motivation

- **Study of long-term evolution of Hamiltonian systems;**
- **Interest in the quick detection and inspection of chaotic layers in the phase space:**
  - Extrapolation of long-term dynamics;
  - Fitting of amplitude-dependent scaling laws;
  - Assess correlation between the existence of large chaotic regions and strong diffusive behaviours;
- **New mathematical tools for quickly probe the chaotic behaviour of initial conditions;**
  - Indicators such as the Fast Lyapunov Indicator and the Frequency Map Analysis are well known in the accelerator field;
  - Other novel tools are available and used in astrophysics, but still not widespread in our field;
  - Interest in assessing the performance of these various indicators
- **GPU-enabled tracking can offer large quantity of data for statistical analysis.**

Overview of Dynamic indicators

Regular and chaotic initial conditions

Given a symplectic map $M(\boldsymbol{x})$, an initial condition $\boldsymbol{x}_0$ is defined as either regular or chaotic depending on the **linear response** of the system to a small perturbation $\boldsymbol{y}_0 = \boldsymbol{x}_0 + \epsilon\boldsymbol{\xi}$. Where $\epsilon\boldsymbol{\xi}$ represents a small displacement. The linear response $\boldsymbol{\Xi}_n(\boldsymbol{x})$ is then defined as

$$\boldsymbol{\Xi}_n(\boldsymbol{x}) = \lim_{\epsilon \to 0} \frac{\boldsymbol{y}_n - \boldsymbol{x}_n}{\epsilon}, \text{ where } \boldsymbol{x}_n = M(\boldsymbol{x}_{n-1}, n-1) \equiv M_n(\boldsymbol{x}).$$

- A **chaotic initial condition**, will feature an **exponential-like** linear response $\boldsymbol{\Xi}_n(\boldsymbol{x}) \approx e^{\lambda_1 n}$, where λ_1 is the positive value **maximal Lyapunov exponent** of the initial condition.
  - For an m dimensional system, each initial condition features a spectrum of λ_m Lyapunov exponents representing different attractors along the orthonormal base of choice.
- Conversely, a **regular initial condition** is characterised by only zero-value Lyapunov exponents.

Detecting chaos via indicators

- To efficiently characterise the chaotic behaviour of an orbit, multiple **chaos indicators** have been developed;
- Chaos indicators inspect specific features of the orbit and provide a numerical evaluation whose value and convergence rate depends on the orbit behaviour;
- The most well known indicator of chaos is the **Fast Lyapunov Indicator** (FLI). The quantity $\frac{FLI}{n}$ provides an estimate of the maximal Lyapunov exponent at a finite time n and reads:

$$\frac{FLI_n(\boldsymbol{x}_0, \boldsymbol{\xi})}{n} = \sum_{i=0}^{n-1} \frac{\ln ||\boldsymbol{y}_i - \boldsymbol{x}_i||}{n}.$$

  And will converge to zero for a regular orbit, and to a positive value for a chaotic orbit.

Other indicators of chaos (1/3)

Many indicators have been developed over time, especially in the field of astrophysics. In our studies, we focused our attention on a selection of 7 different indicators (including FLI)

- **Lyapunov Error** (LE); instead of estimating the linear response of the system on a single displacement like FLI, it considers the trace of the covariance matrix of the full **tangent map** $\mathrm{L}_n(\boldsymbol{x}) = DM(\boldsymbol{x}_{n-1}; n-1) \dots DM(\boldsymbol{x}_0; 0)$, that is

$$LE_n(\boldsymbol{x}) = \sqrt{\mathrm{Tr}(\mathrm{L}_n^T(\boldsymbol{x})\mathrm{L}_n(\boldsymbol{x}))}.$$

- **Fast Lyapunov Indicator with Birkhoff weights** (FLI^{WB}); we can make use of the superconvergence properties provided by the Birkhoff weights to achieve convergence rates faster than FLI, the original FLI sum then reads

$$FLI_n^{WB}(\boldsymbol{x}_0, \boldsymbol{\xi}) = \sum_{i=0}^{n-1} w\left(\frac{i}{n}\right) \ln\left|\left|\boldsymbol{y}_i - \boldsymbol{x}_i\right|\right|; \quad \text{with} \quad \mathrm{w(t)} \coloneqq \begin{cases} \exp\left[-\dfrac{1}{t(1-t)}\right], & \text{for } t \in (0,1) \\ 0, & \text{for } t \notin (0,1) \end{cases}.$$

Other indicators of chaos (2/3)

- **Mean Exponential Growth of Nearby Orbits** $(MEGNO)$;
  - Reduces the fluctuations of a "direct" evaluation of an indicator such as FLI or LE by means of a **double-time average filter**.
  - The resulting indicator reads (for the case of LE):

$$MEGNO_n\big(LE(\boldsymbol{x})\big) = \left\langle\left\langle t\,\frac{d\log LE_n(\boldsymbol{x})}{dt}\right\rangle\right\rangle \quad \text{where} \quad \langle f(t)\rangle = \frac{1}{t}\int_0^t f(t')dt$$

- **Reversibility Error Method** (REM);
  - Uses the **numerical uncertainty** as a tool to evaluate the orbit chaotic behaviour.
  - By performing a **tracking and backtracking** of n iterations, we can use the resulting displacement from the original initial condition as a measure of chaos.
    - A regular orbit will have a displacement following a power law.
    - A chaotic orbit will instead exhibit an exponential increase.

Other indicators of chaos (3/3)

- **Generalized Alignment Index** $(GALI)$;
  - $GALI^{(k)}$ considers the evolution of $\boldsymbol{k}$ **initial orthonormal displacements**, then, evaluates the volume of the parallelotope whose sides are the **normalised images of the evolved displacements**.
    - For a chaotic orbit, these displacements will eventually all **align towards the maximal Lyapunov exponent** (i.e. volume zero);
    - For a regular orbit, the volume of the parallelotope **either stays constant or follows a power law depending on** $\boldsymbol{k}$.
- **Frequency Map Analysis** (FMA);
  - Well-established in accelerator physics.
  - Evaluates the variation of the fundamental frequency (i.e. the tune) over different time intervals.
    - We evaluate the tune variation on the $x - p_x$ and $y - p_y$ plane over the time intervals $\left[0, \frac{n}{2}\right]$ and $\left[\frac{n}{2}, n\right]$.
  - Large variations in tune can be related to chaotic behaviour.

Application to the modulated Hénon map with octupolar kicks

The modulated Hénon map with octupolar kicks

- 4d polynomial time-dependent symplectic map;
- Combination of fixed quadratic nonlinearities and cubic ones regulated by μ;
- Double rotation matrix with "SPS-like" modulations with amplitude regulated by ε (the harmonics ε_k have an order of magnitude of 10^{-4});

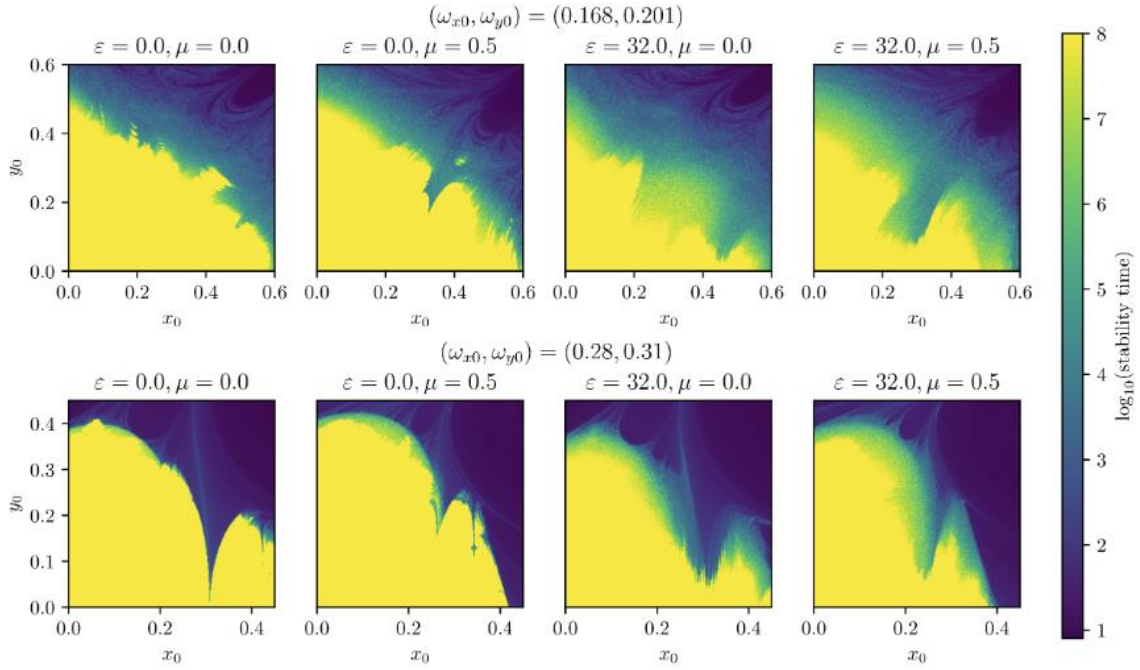

Survival plot of the Hénon map ($n_{\max} = 10^8$)

$$\begin{pmatrix} x_{n+1} \\ p_{x,n+1} \\ y_{n+1} \\ p_{y,n+1} \end{pmatrix} = R(\omega_{x,n}, \omega_{y,n}) \times \begin{pmatrix} x_n \\ p_{x,n} + x_n^2 - y_n^2 + \mu\left(x_n^3 - 3x_n y_n^3\right) \\ y_n \\ p_{y,n} - 2x_n y_n + \mu\left(y_n^3 - 3y_n x_n^3\right) \end{pmatrix}$$

$$\omega_{x,n} = \omega_{x,0}\left(1 + \varepsilon \sum_{k=1}^{m} \varepsilon_k \cos\left(\Omega_k n\right)\right)$$

$$\omega_{y,n} = \omega_{y,0}\left(1 + \varepsilon \sum_{k=1}^{m} \varepsilon_k \cos\left(\Omega_k n\right)\right)$$

k	Ω_k	$10^4 \epsilon_k$
1	$2\pi/868.12$	1.000
2	$2\Omega_1$	0.218
3	$3\Omega_1$	0.708
4	$6\Omega_1$	0.254
5	$7\Omega_1$	0.100
6	$10\Omega_1$	0.078
7	$12\Omega_1$	0.218

Implementation of chaos indicators

- Straightforward implementation on GPU architectures;
- Available **analytical expression** of the tangent map $DM(\boldsymbol{x})$
  - Enables direct evaluation of $\mathrm{L}_n(\boldsymbol{x})$;
  - Possible to explore multiple displacements with no extra computational cost;
- Possible to reach high iteration times ($n = 10^8$)

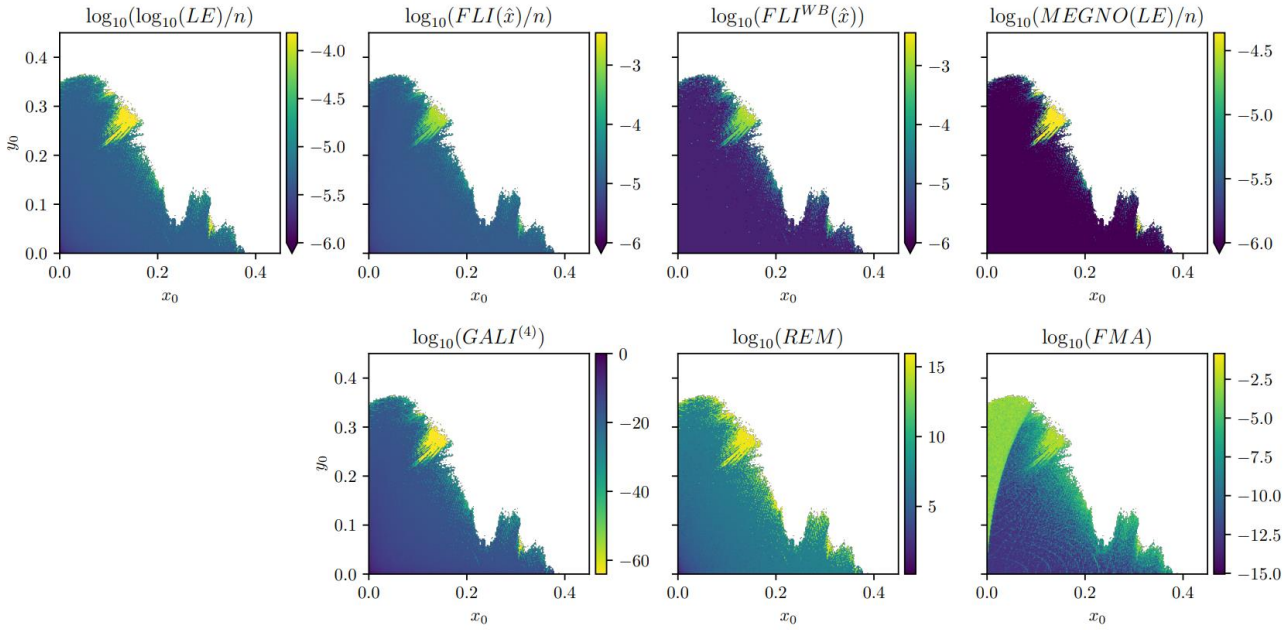

Various dynamic indicators on a Hénon map ($n = 10^5$)
Simulation parameters: $(\omega_{x0}, \omega_{y0}) = (0.28, 0.31), \varepsilon = 32.0, \mu = 0.5$

Convergence of dynamic indicators over time

- Dynamic indicators have the tendency to create a **bimodal distribution** over time (with the exception of FMA, which tends to a tri-modal distribution)
  - One populated cluster of regular initial conditions;
  - A minor cluster or spread of values given by the chaotic initial conditions;
- From this, we can define an “agnostic” classification algorithm;
- Question: which indicator is the “best performing” in distinguishing regimes?

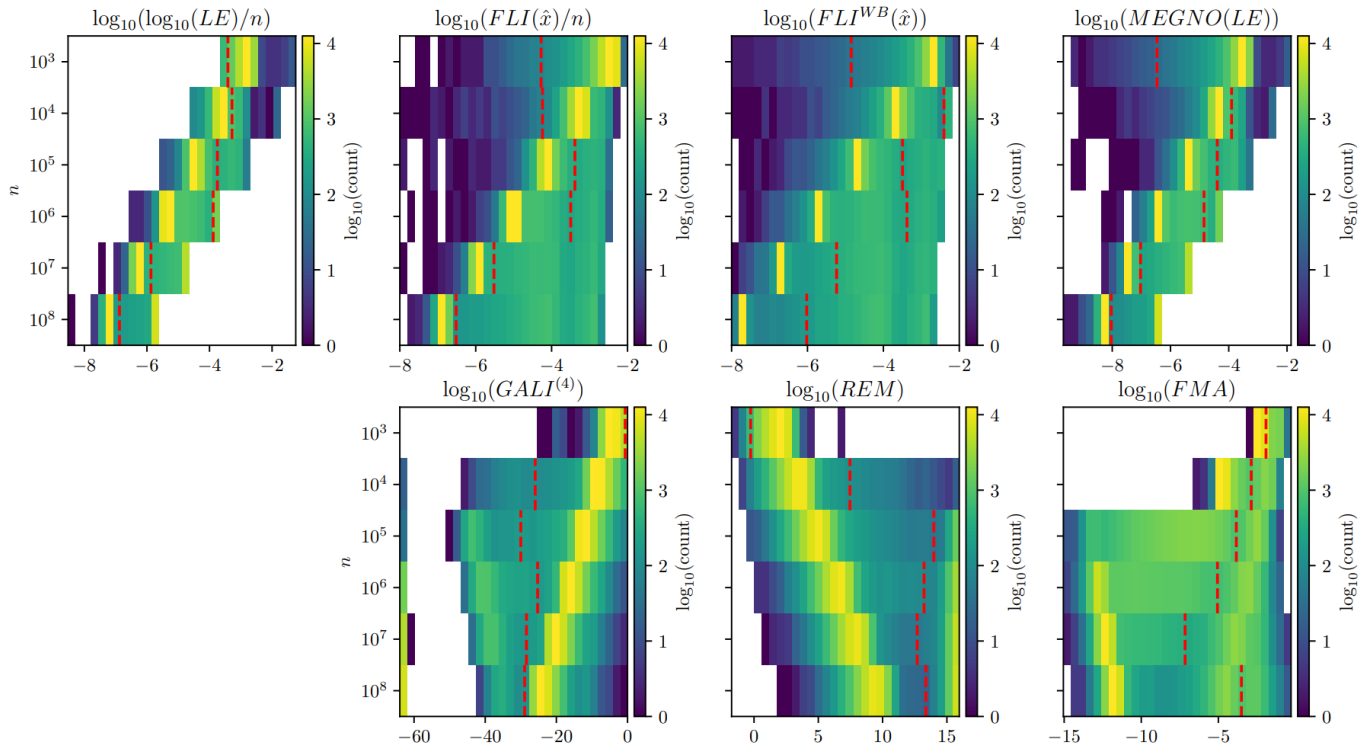

Value distribution over time of dynamic indicators on a Hénon map
Simulation parameters: $(\omega_{x0}, \omega_{y0}) = (0.28, 0.31), \varepsilon = 32.0, \mu = 0.5$

Defining the classification performance

- "Agnostic" thresholding algorithm for detecting the two main distribution modes;
  - Returns a binary classification threshold regular/chaotic;
- Kernel Density Estimate (KDE) with progressively smaller bandwidth
  - Bandwidth reduction stops when the fluctuations in the distributions become significant;
- For the specific case of FMA, the algorithm looks for three modes.

Overview of KDE based thresholding algorithm for REM (top) and FMA (bottom)

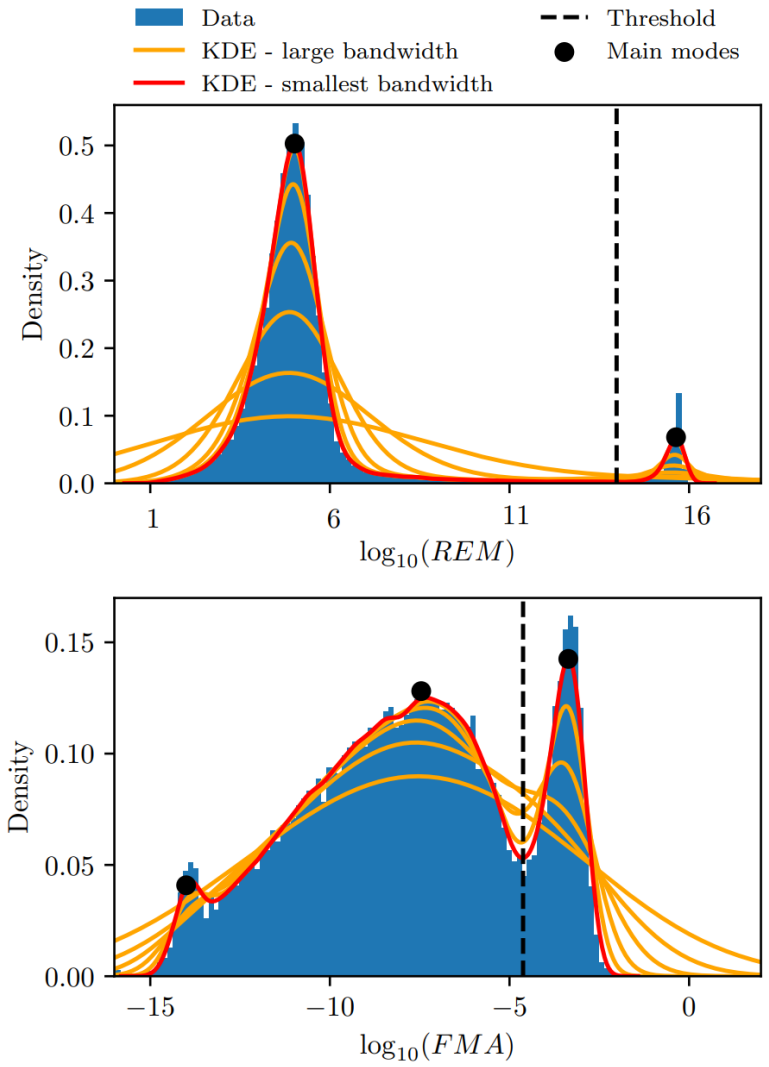

Defining a Ground Truth (GT)

- From the algorithm, we define a Ground Truth (GT) using the $\log_{10}(\log_{10}(LE)/n)$ value with $n = 10^8$;
- Well defined distinction between chaotic and regular initial conditions;
- A good-performing indicator will reconstruct the GT at lower n values. Conversely, a bad-performing indicator will require higher n values.

Visualization of GT construction

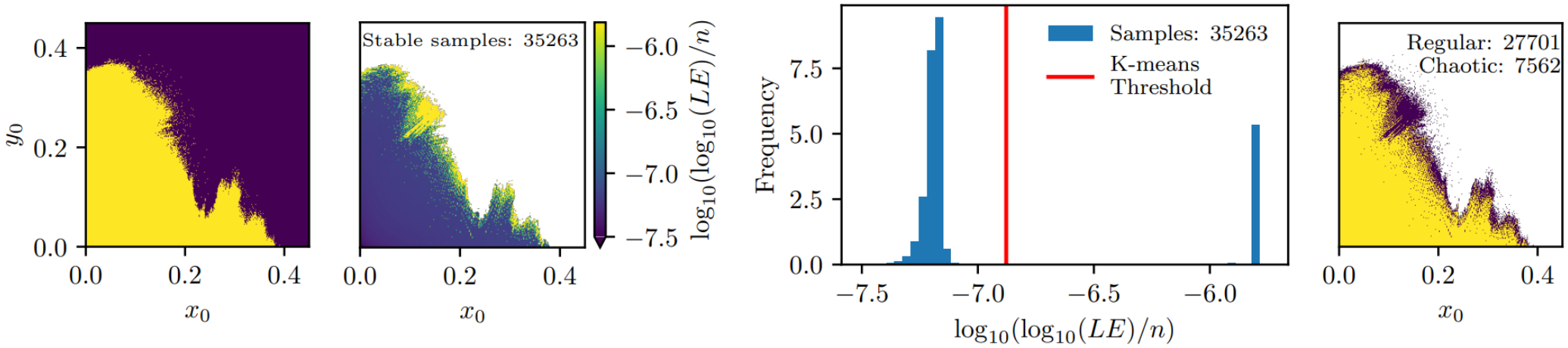

Performance overview

- We evaluate as performance metric the **accuracy** (i.e. correct classifications / total samples) of the indicator in reconstructing the GT;
- In general, REM and $GALI^{(4)}$, show the best performance;
- Other Lyapunov-related indicators tend to achieve comparable performances only at higher times;
- FMA shows to be strongly dependent from tune, modulation and resonances, as it detects them along with chaotic behaviour.

Accuracy evolution over time for the various dynamic indicators

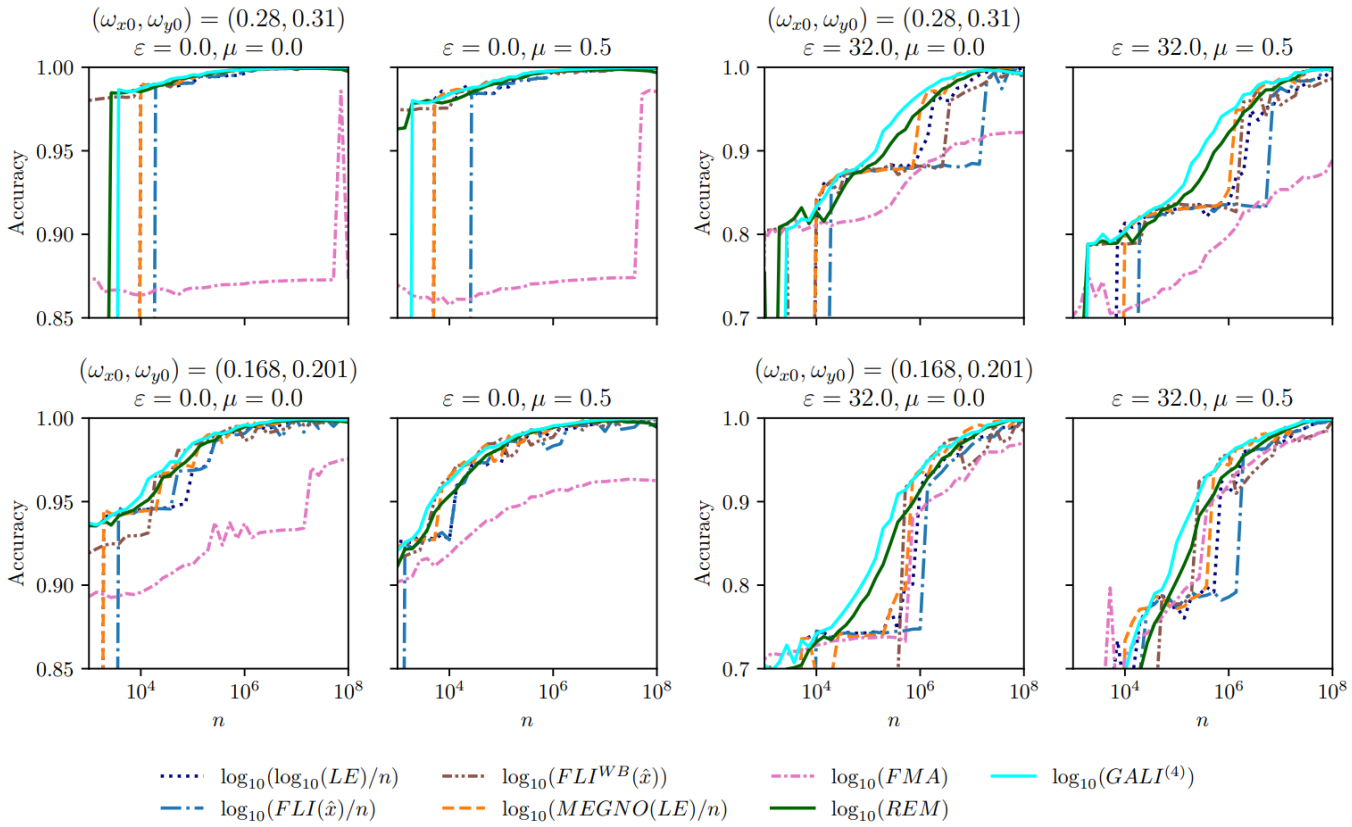

Improved convergence of FLI with Birkhoff weights

- Birkhoff weights have been successfully applied for the fast evaluation of tunes;
- In literature, we have examples (without proof) of improved FLI evaluation thanks to Birkhoff weights;
- We have confirmed the result on the Hénon map case, and observed both faster convergence and more narrow distribution modes;
- Both these elements provided better performances in reconstructing the GT;

Simulation parameters: $(\omega_{x0}, \omega_{y0}) = (0.28, 0.31), \varepsilon = 32.0, \mu = 0.5$

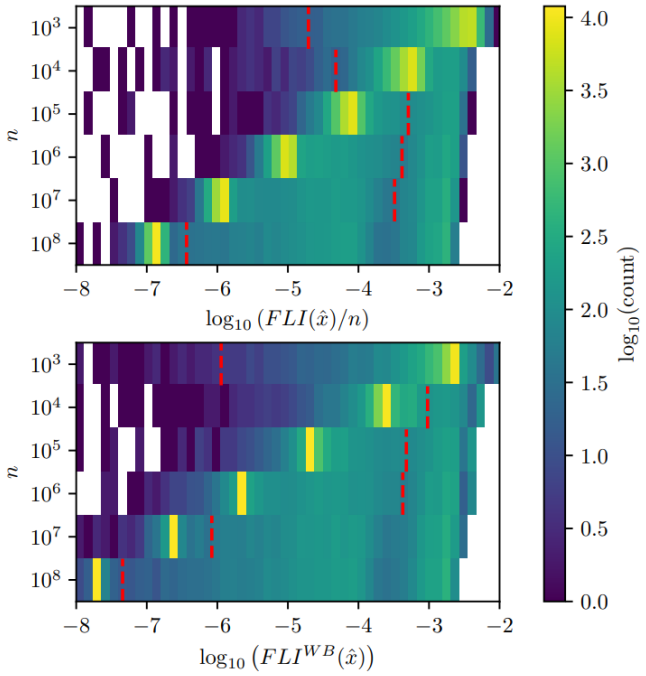

Value evolution over time

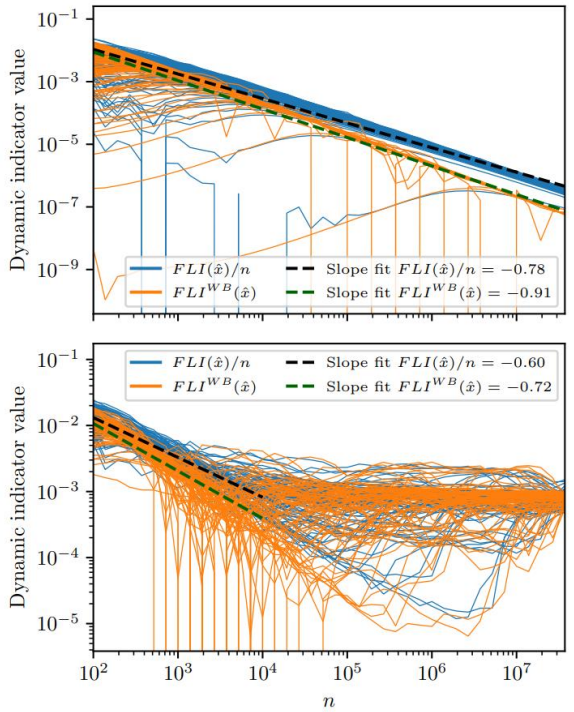

(top) ensemble of regular initial conditions.
(bottom) ensemble of chaotic initial conditions.

Final considerations from the Hénon map

From the analysis of the Hénon map, we have learned the following things:

- REM and $GALI^{(k)}$ indicators seem to provide the best performance in fast detection of chaos;
- FLI^{WB} seems to be a valid improvement over the regular FLI. Therefore it's preferable for estimating the maximal Lyapunov exponent.
- If we are interested in chaos detection only, FMA might be affected by resonance lines and modulation effects.

We can now transport this knowledge to more realistic accelerator lattices.

Application to a realistic HL-LHC lattice

HL-LHC characteristics

- HL-LHC v1.4 Beam 1 optics;
- Colliding beams at top energy;
- No beam-beam interactions;
- Two different magnet noise realisations
  - Out of the table of 60 seeds, we picked the ones which scored, respectively, the best and worst Dynamic Aperture at $n = 10^5$ turns.
- Three different values of ζ_0
  - Reference orbit, half of the bucket, near the bucket separatrix.

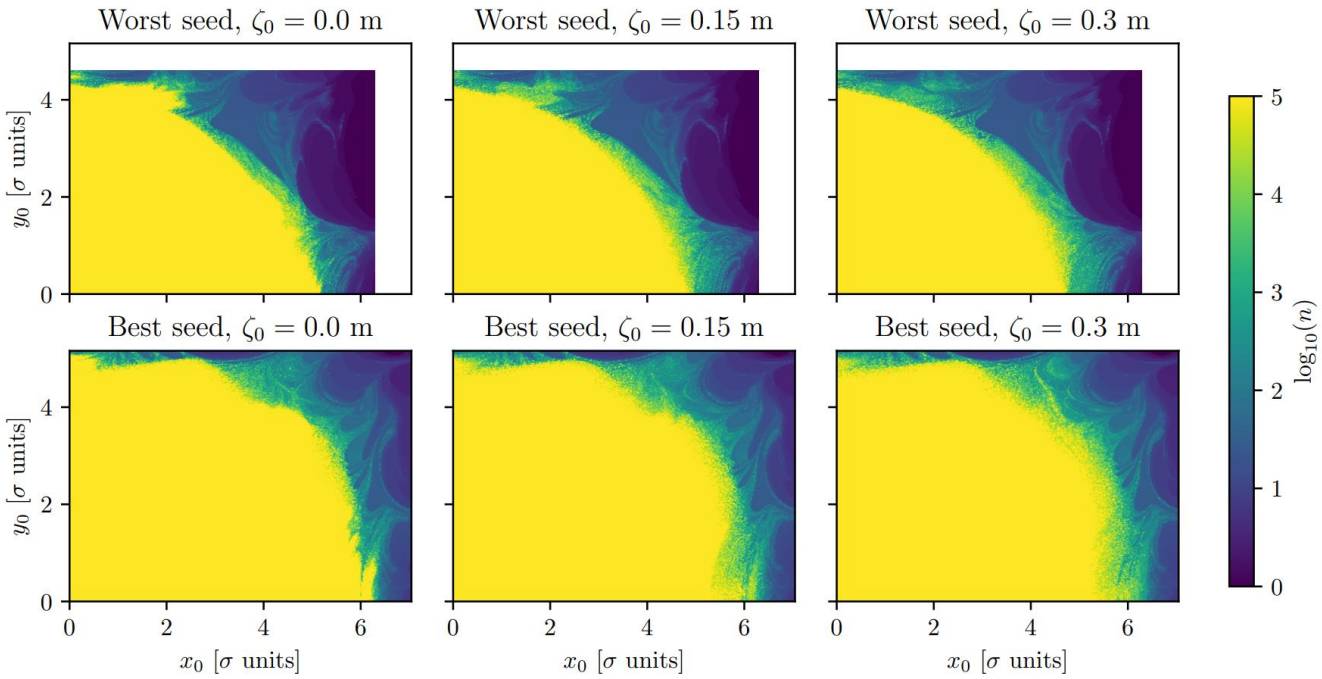

Survival plot of HL-LHC ($n_{\max} = 10^5$)

Evaluating chaos indicators without a tangent map expression

- Current tools do not offer analytical expressions of the tangent map of realistic lattices;
- To overcome this issue, we implemented the "shadow particle" method to numerically estimate it for a given displacement $\epsilon\boldsymbol{\xi}$:
  - Given an initial condition $\boldsymbol{x}_0$ to track, also track $\boldsymbol{y}_0 = \boldsymbol{x}_0 + \epsilon\boldsymbol{\xi}$.
  - Every τ turns, renormalize the distance between $\boldsymbol{y}$ and $\boldsymbol{x}$ to ϵ.
- Straightforward implementation for evaluating both linear response and evolution of the displacement direction over time.

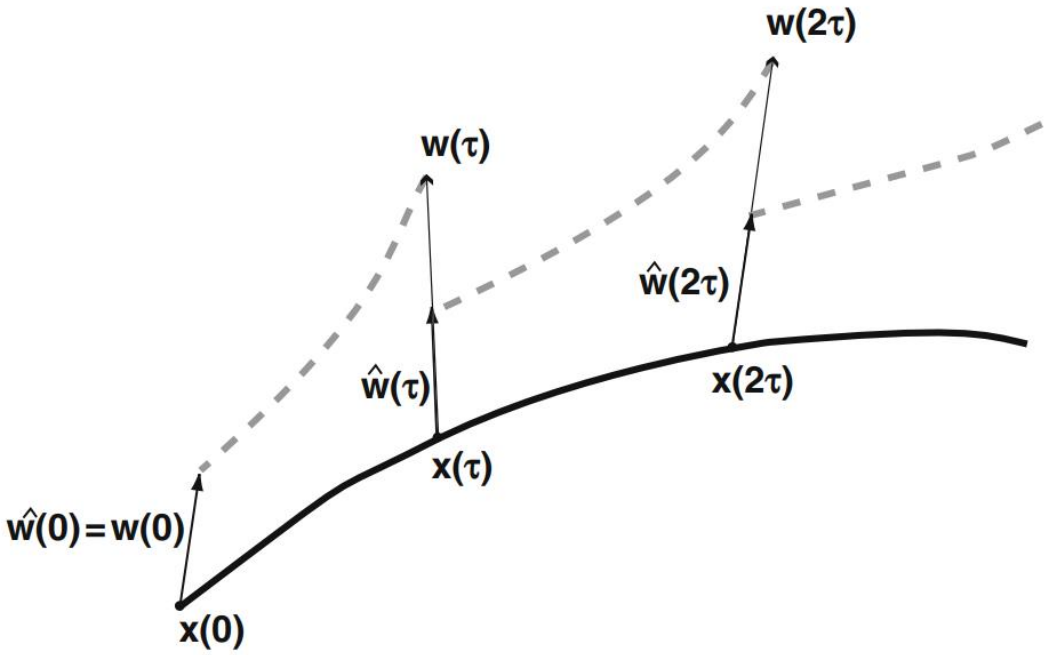

Sketch of the ghost particle method

Implementation on Xsuite

- Straightforward GPU single-particle tracking implementation;
- Easy to implement “custom” normalisation of ghost particles;
- GPUs enable scale-up of initial conditions and consequent statistical analysis;
  - Tracking 10^5 particles up to 10^5 turns takes ~2.5h on a Nvidia Tesla A100;
- We inspected FLI/n, FLI^{WB}, REM, $GALI^{(k)}$, and FMA.

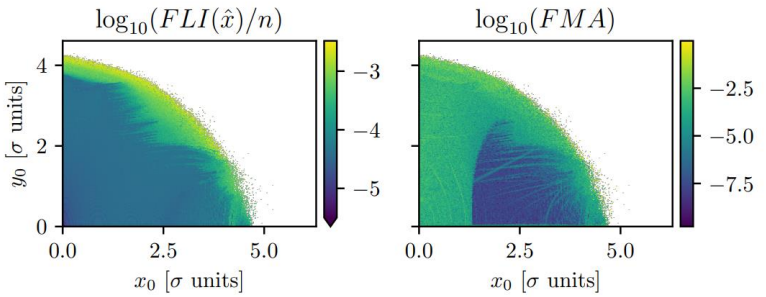

Dynamic indicators evaluated on a HL-LHC lattice ($n = 10^5$)
Worst seed, $\zeta_0 = 0.3$m

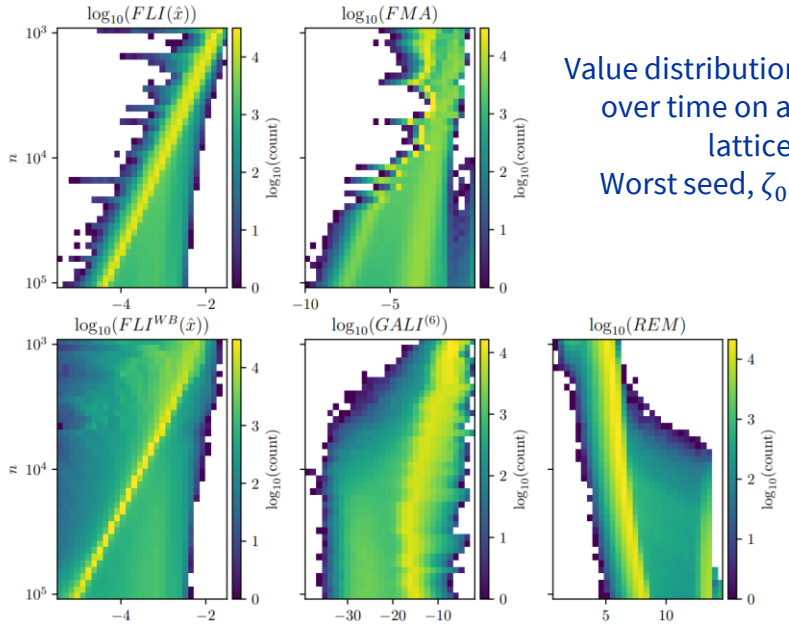

Value distribution evolution over time on a HL-LHC lattice
Worst seed, $\zeta_0 = 0.3$m

Longitudinal dynamics and FMA

- Different values of ζ_0 yield different levels of longitudinal dynamics;
- Larger chaotic regions when ζ_0 is closer to the bucket separatrix;
- FMA shows a behaviour similar to the one observed on the Hénon map
  - Affected not only by chaos, but also by resonances;
  - Differences in structures detected, when compared to FLI^{WB}, increase with ζ_0.

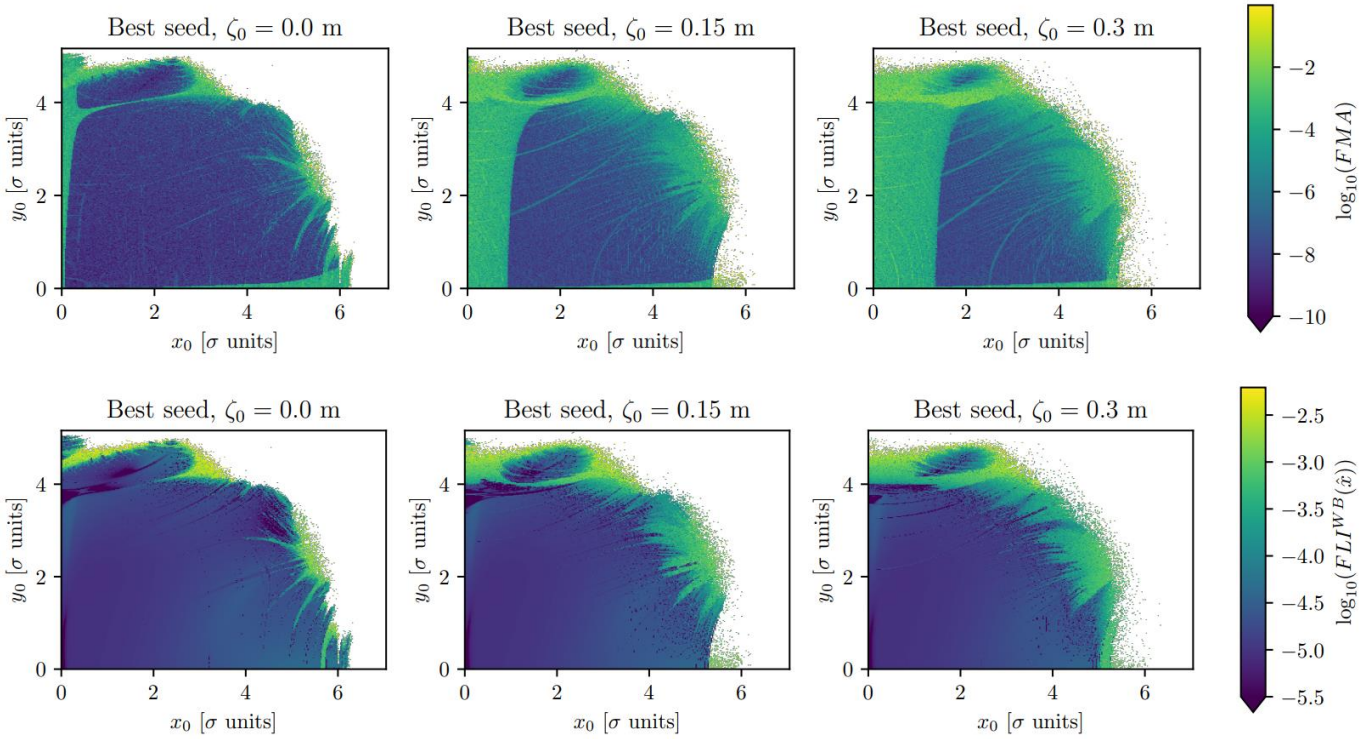

Graphic comparison between FMA (top row) and FLI^{WB} (bottom row). $n = 10^5$

Inspecting the Lyapunov Time and the Stability Time

- We are interested in investigating the mean Lyapunov Time T_L and the mean Stability Time T_s at different amplitudes
  - T_L being the inverse of the maximal Lyapunov exponent (infinite when λ_1=0, finite when λ_1 has positive value);
  - T_s being the time at which an initial condition is lost (with $n_{\max} = 10^5$);
- We consider a moving average with $\Delta r = 0.2\sigma$;

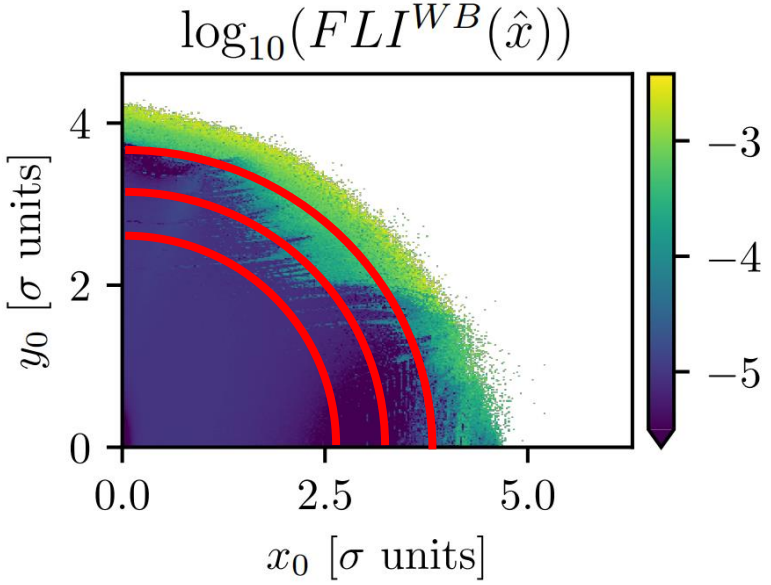

Sketch of different amplitudes over which the mean value is measured

Inspecting the Lyapunov Time and the Stability Time

- Both T_L and T_s measurements have an inevitable "saturation" at low amplitudes due to the limited iteration number $n_{\max} = 10^5$;
- T_s follows a clear Nekhoroshev-like decay law

$$T = T_0 \exp\left[-\left(\frac{I_*}{I_0}\right)^{\frac{1}{2\kappa}}\right]$$

- T_L displays a similar evolution, also very dependent on the value of ζ_0
  - T_L might be an interesting tool for "deeper" inspections of the Nekhoroshev character of the system.

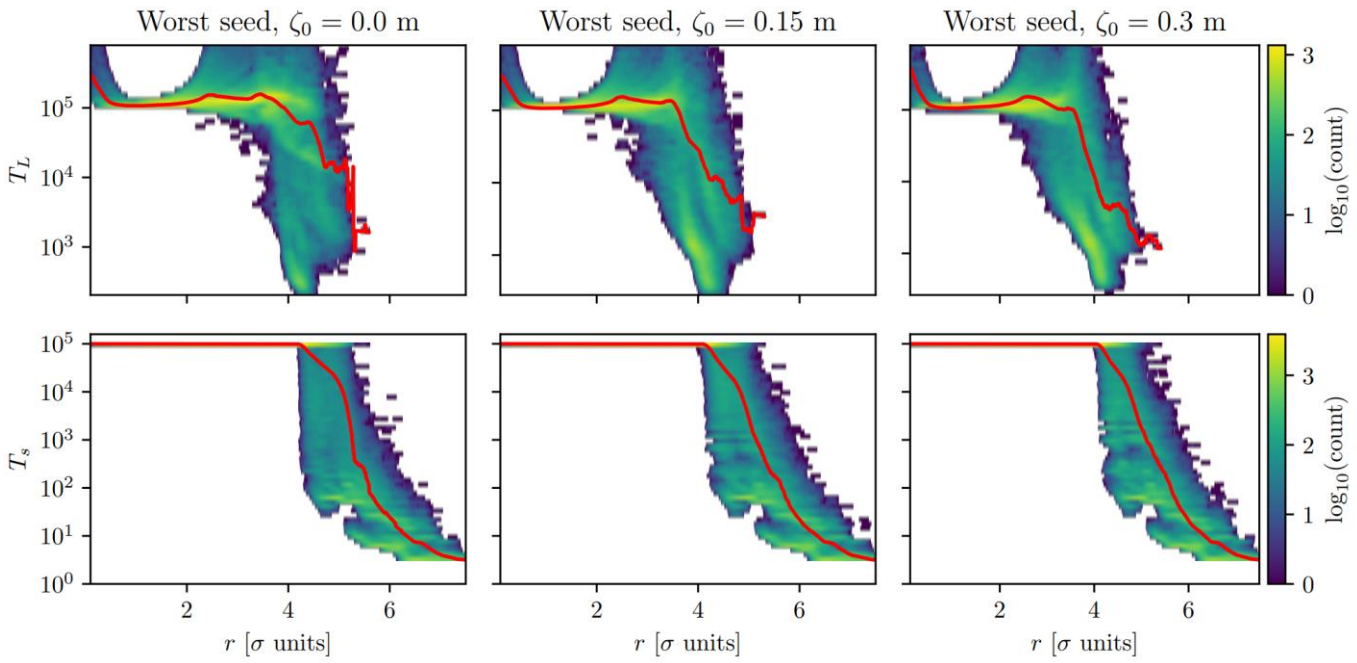

Resulting mean from the moving average at different amplitudes.
The colormap represents the value distribution observed at the specific radius.

Investigating the scaling laws

- To pick the optimal slice of data to fit (no saturated data and no excessive discarding), we fit multiple slices with cuts at increasingly higher amplitudes;
  - The final slice choice is made by minimising the reduced χ^2;
- Good fitting performance for all cases, with the exception of T_L fit when $\zeta_0 = 0$;
  - Case with the "smallest" chaotic regions in the phase space;
  - Might be solvable with finer sampling.

Visualization of fitting procedure $\zeta_0 = 0.3$m

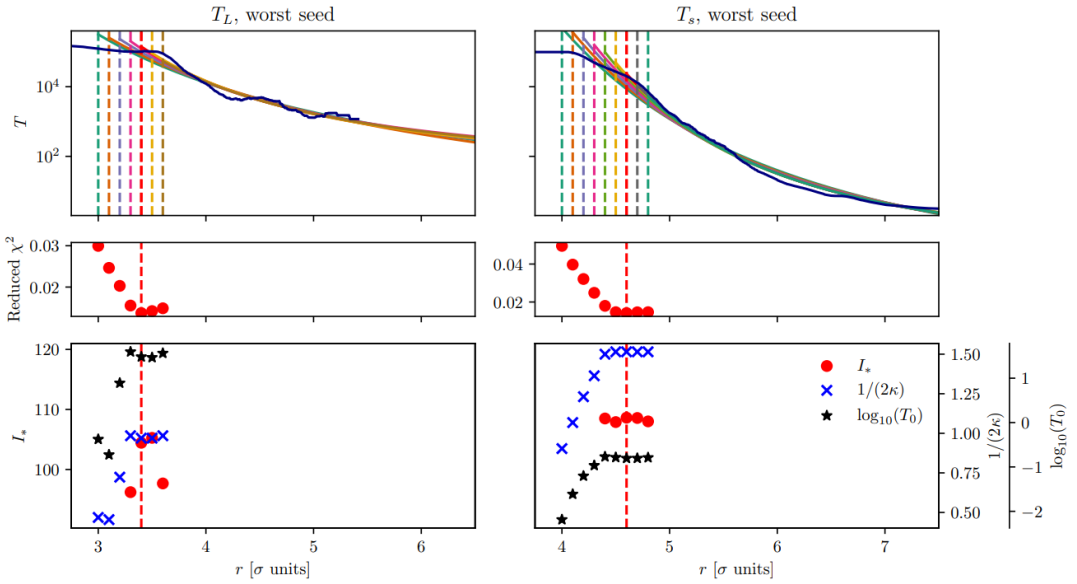

Fit results

T_s fit		$\zeta_0 = 0.0$ m	$\zeta_0 = 0.15$ m	$\zeta_0 = 0.3$ m
Worst seed	$1/(2\kappa)$	2.94 ± 0.02	3.0 ± 0.2	3.03 ± 0.08
	I_*	131 ± 2	119 ± 7	109 ± 5
	$\log_{10}(T_0)$	-1.23 ± 0.04	-0.95 ± 0.08	-0.81 ± 0.06
	Red. χ^2	0.069	0.021	0.014
Best seed	$1/(2\kappa)$	2.9997 ± 0.0004	3.03 ± 0.07	3.00 ± 0.08
	I_*	220 ± 40	208 ± 28	206 ± 23
	$\log_{10}(T_0)$	-2.2 ± 0.3	-1.9 ± 0.3	-1.819 ± 0.004
	Red. χ^2	0.086	0.055	0.028
T_L fit		$\zeta_0 = 0.0$ m	$\zeta_0 = 0.15$ m	$\zeta_0 = 0.3$ m
Worst seed	$1/(2\kappa)$	1 ± 3	1.88 ± 0.01	1.9 ± 0.1
	I_*	2500 ± 1600	100 ± 40	104 ± 31
	$\log_{10}(T_0)$	-3 ± 17	1.9 ± 0.3	1.5 ± 0.3
	Red. χ^2	0.049	0.010	0.014
Best seed	$1/(2\kappa)$	1.5 ± 1.0	2.94 ± 0.08	2.7 ± 0.1
	I_*	1700 ± 400	108 ± 25	98 ± 27
	$\log_{10}(T_0)$	-4 ± 5	1.1 ± 0.3	1.5 ± 0.3
	Red. χ^2	0.018	0.003	0.016

On the relation between T_L and T_S

- In the work of Morbidelli et al., the existence of a relation between T_L and T_S is discussed.
- Although the relation is found to be deeply model dependent, the authors distinguish two regimes:
  - Resonance overlapping regime $T_S \sim T_L^{\beta}$;
  - Nekhoroshev regime $T_S \sim \exp(T_L)$;
- If we assume both T_L and T_S follow a Nekhoroshev scale-law, we can derive

$$\frac{T_{\mathrm{s}}}{T_{0,\mathrm{s}}} = \exp\left[\left(\frac{I_{*,\mathrm{s}}}{I_{*,\mathrm{L}}}\right)^{1/2\kappa_{\mathrm{s}}}\left(\log\frac{T_{\mathrm{L}}}{T_{0,\mathrm{L}}}\right)^{\kappa_{\mathrm{L}}/\kappa_{\mathrm{s}}}\right]$$

- If $\frac{\kappa_L}{\kappa_S} = 1$, we recover a polynomial relation $T_S = \alpha T_L^{\beta}$;
- If $\frac{\kappa_L}{\kappa_S} \neq 1$, we have the relation in the form

$$T_S = \alpha \exp\left(\beta \log\left(\frac{T_L}{T_{0,L}}\right)^{\kappa_L/\kappa_S}\right);$$

Relation T_s, T_L		$\zeta_0 = 0.0$ m	$\zeta_0 = 0.15$ m	$\zeta_0 = 0.3$ m
Worst seed	κ_L/κ_s	2 ± 6	1.56 ± 0.08	1.56 ± 0.09
	α	$(5.9 \pm 0.5) \times 10^{-2}$	$(1.1 \pm 0.2) \times 10^{-1}$	$(1.6 \pm 0.2) \times 10^{-1}$
	β	$(1.6 \pm 3.1) \times 10^{-4}$	1.4 ± 1.6	1.1 ± 1.0
Best seed	κ_L/κ_s	2.0 ± 1.3	1.03 ± 0.03	1.13 ± 0.06
	α	$(0.7 \pm 0.5) \times 10^{-2}$	$(1.2 \pm 0.7) \times 10^{-2}$	$(1.51 \pm 0.01) \times 10^{-2}$
	β	$(2.2 \pm 2.0) \times 10^{-3}$	7 ± 6	9 ± 8

Relation values based on Nekhoroshev fit results (considering $\frac{\kappa_L}{\kappa_S} \neq 1$)

$GALI^{(k)}$ indicators for inspecting tori geometry (ongoing)

- When picking $k < 6$ (i.e. the number of dimensions of the system), one can choose different combinations of displacement directions;

- A chaotic initial condition will have a decaying $GALI$ value over time following

$$GALI^{(k)} \propto \exp\left[-t\left((\lambda_1 - \lambda_2) + (\lambda_1 - \lambda_3) + \cdots + (\lambda_1 - \lambda_k)\right)\right]$$

- Conversely, a regular initial condition will follow

$$GALI^{(k)} \propto \begin{cases} \text{constant} & \text{if } 2 \leq k \leq N \\ \frac{1}{t^{2(k-N)-m}} & \text{if } N < k \leq 2N \text{ and } 0 \leq m < k - N \\ \frac{1}{t^{k-N}} & \text{if } N < k \leq 2N \text{ and } m \geq k - N \end{cases}$$

with m dependent on the tori geometry. This coefficient might give insights on the phase space structure of the system.

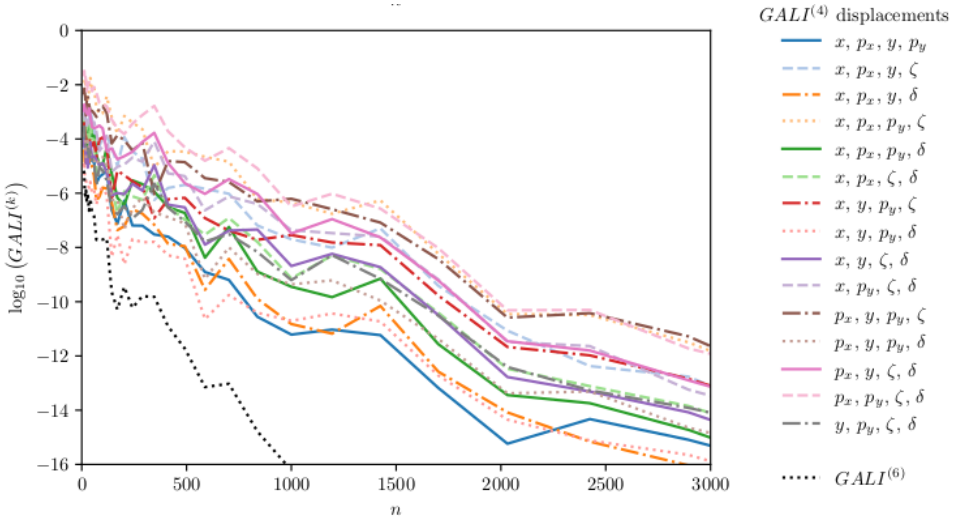

Evolution of $GALI^{(k)}$ with k=4, 6 for an ensemble of chaotic initial conditions for every possible set of displacement choices.

Final considerations and future work

- GPU performance gain and the usage of novel dynamic indicators offer interesting opportunities for probing the chaotic behaviour of accelerator lattices;
- Knowledge obtained from the Hénon map can be easily transposed to realistic lattices;
- Inspecting the Lyapunov time T_L can provide insights on the Nekhoroshev character of a system;

Future work:

- Dedicated analysis of $GALI^{(k)}$ indicators on regular orbits for inspecting tori geometry;
- Finer sampling of initial conditions at higher turns ($n_{\max} = 10^6$);
- Tracking of chaotic initial conditions for dedicated diffusion measurements;
- Code release on Xsuite.